



New insights into the 2021 La Palma eruption degassing processes from direct-sun spectroscopic measurements

Noémie Taquet^{1,2,3}, Thomas Boulesteix², Omaira García¹, Robin Champion⁴, Wolfgang Stremme⁵, Sergio Rodríguez⁶, Jessica López-Darias⁶, Carlos Marrero¹, Diego González-García^{7,8}, Andreas Klügel⁹, Frank Hase¹⁰, M. Isabel García⁶, Ramón Ramos¹, Pedro Rivas-Soriano¹, Sergio León-Luis^{1,3,11}, Virgilio Carreño¹, Antonio Alcántara¹, Eliezer Sépulveda^{1,3}, Celia Milford¹, Pablo González-Sicilia^{1,3}, Carlos Torres¹

¹ Izaña Atmospheric Research Center (IARC), State Meteorological Agency of Spain (AEMET), Tenerife, Spain

² Consejo Superior de Investigaciones Científicas, Volcanology Research Group, IPNA-CSIC, Tenerife, Canary Islands, Spain

³ TRAGSATEC, Madrid, Spain

⁴ Universidad Nacional Autónoma de México, Instituto de Geofísica, Mexico City, Mexico

⁵ Universidad Nacional Autónoma de México, Instituto de Ciencias de la Atmósfera y Cambio Climático, Mexico City, Mexico

⁶ Consejo Superior de Investigaciones Científicas, Group of Atmosphere, Aerosols and Climate, IPNA CSIC, Tenerife, Canary Islands, Spain

⁷ Institute of Earth System Sciences (Section of Mineralogy), Leibniz University of Hannover, Hannover, Germany

⁸ Department of Mineralogy and Petrology, Universidad Complutense de Madrid, Madrid, Spain

⁹ Department of Geosciences, University of Bremen, Bremen, Germany

¹⁰ Institute for Meteorology and Climate Research, Karlsruhe Institute of Technology, Karlsruhe, Germany

¹¹ Departamento de Física, Universidad de La Laguna, San Cristóbal de La Laguna, Santa Cruz de Tenerife, Spain

Correspondence to: Noémie Taquet (noemi.taquet@gmail.com) and Omaira Garcia (ogarcia@aemet.es)

Abstract. During the 2021 La Palma eruption, both existing and newly deployed air quality and atmospheric monitoring networks in the Canary Islands (Spain) played a crucial role in supporting decision-making for public safety and enhancing the understanding of the crisis. In this study, we report direct-sun measurements using low (EM27/SUN) and high (IFS-125HR) spectral resolution Fourier Transform InfraRed (FTIR) spectrometers located up to ~140 km away from the volcano and contributing to key atmospheric global networks. In La Palma, the EM27/SUN was combined with a Differential Optical Absorption Spectroscopy (DOAS) instrument. We present new FTIR retrieval methods to derive the SO₂, CO₂, CO, HF, HCl relative abundance in the volcanic plume from both low- and high- resolution solar absorption spectra. We derived SO₂ volcanic emission fluxes from the Sentinel-5P TROPOspheric Monitoring Instrument (TROPOMI) and estimated the emission fluxes of the other volcanic species over the whole eruption. We estimate the volcanic emission to the atmosphere for SO₂, CO₂, HCl, HF and CO to be 1.8±0.2Mt, 19.4±1.8Mt, 0.05±0.01Mt, 0.013±0.002Mt and 0.123±0.005Mt, respectively. We show a good agreement between these estimates and the degassing balance derived from a petrologic approach. This eruption produced emissions that compare directly with annual anthropogenic emissions at different spatial scales. This study demonstrates the feasibility of using existing atmospheric FTIR and DOAS global networks to monitor volcanic plumes composition more than 100 km away, and is of relevance for volcanological monitoring and research during volcanic crises.

1. Introduction

Volcanic emissions of greenhouse gases and pollutants remain poorly constrained due to the limited number of volcanoes well monitored for gas emissions. The present knowledge relies on either partial records at permanent stations or on discrete campaigns of measurements during eruptive crises. Characterizing volcanic



45 degassing processes is critical for improving our understanding of the multi-species volcanic gas emissions
46 across various geodynamic settings and their long- and short-term impact on the atmospheric composition.

47 The abundance and composition of dissolved volatiles control the buoyancy and viscosity of magmas, making
48 these a primary driver of eruptive dynamism and duration. Water (H₂O) and carbon dioxide (CO₂) are the most
49 abundant species in volcanic degassing, followed by sulphur dioxide (SO₂) and halogen-derived species (mainly
50 halides). Due to their contrasted solubility in magma, which depends mainly on pressure, temperature and redox
51 conditions (Gennaro et al., 2020; Cassidy et al., 2022), CO₂ and H₂O are among the deepest exsolved gas
52 species, followed by SO₂ and halogens in sub-surface. The exploration of their pre- and co-eruptive relative
53 abundance can reveal critical information on pressurisation of the magma plumbing system, as well as on ascent
54 rates and volatile exsolution pathways (Voigt et al., 2014; Taquet et al., 2019). The temporal evolution of the
55 CO₂/SO₂ ratio and halogen-derived species-to-SO₂ ratios in volcanic plumes have often been used to infer the
56 respective contribution of deep to shallow magmatic processes in the transitions in eruptive dynamism such as
57 changes in the bubble contents in the magma chamber, replenishment, magma batches mixing or fractional
58 crystallisation (Harris and Rose, 1996; Shinohara et al., 2003, 2008; Werner et al., 2012; La Spina et al., 2015).
59 Volcanic plume compositions are generally confronted with geophysical observations (structural and seismic)
60 and degassing models to infer the degassing processes, melt evolution and architecture of the plumbing system.
61 Combining surface gas monitoring and petrological data such as composition of matrix, melt and fluid
62 inclusions (thereafter MI and FI, respectively) is critical to obtain complete degassing balance and may also
63 shed light on dynamic aspects of magmatic and volcanic processes and contribute to comprehensive conceptual
64 models of a given eruption.

65 The 2021 La Palma fissure eruption (from 19 September to 14 December 2021, VEI 3), called
66 Tajogaite, was the first subaerial eruption in 50 years in the Canary Islands archipelago and thus the first
67 opportunity to directly assess the amount and composition of volcanic degassing during an eruption in Canary
68 Islands (Burton et al., 2023). It was preceded by up to 12 low intensity seismic swarms between October 2017
69 and September 2021, occurring in depths between 20 and 30 km, without evidence of surface deformation
70 (Torres-Gonzalez et al., 2020; Mezcuca and Rueda, 2023). Some of these seismic swarms were accompanied by
71 changes in flux or composition of trace gases (CO₂, He, Rn) in soil or at the Dos Aguas cold spring located in
72 the Caldera de Taburiente to the north (Torres-Gonzalez et al., 2020; Padrón et al., 2022). These observations
73 were interpreted as evidence of magma migration from a deeper upper mantle reservoir to a shallower sub-
74 crustal reservoir (Padrón et al., 2022). On 11 September 2021, a new seismic swarm occurred at ~10 km depth
75 and intensified over the following days, accompanied by ground inflation reaching 30 cm (De Luca et al., 2022).
76 Subsequently, the seismicity migrated towards the surface and the Tajogaite eruption started on 19 September
77 2021. Several craters opened and grew along a NW-SE eruptive fracture (Muñoz et al., 2022) on the western
78 flank of the Cumbre Vieja Ridge (CVR). The eruption exhibited simultaneously multiple eruptive styles at
79 various summital and flank vents, including more than 100 m-high hawaiian lava fountains, strombolian
80 spattering activity, ash venting, vulcanian explosions and significant effusive activity. Over the 85 days of its
81 activity, it produced a $\sim 1.8 \times 10^8$ m³ lava flow field (Civico et al., 2022) extended over an area of 12 km², and a
82 tephra blanket with a total estimated volume of $\sim 2.3 \times 10^7$ m³ (Bonadonna et al., 2022), provoking the
83 evacuation of several thousands of people and the destruction of ~3000 buildings (Copernicus EMSR546,
84 PEVOLCA reports). During the course of the eruption, volcanic plumes were injected between 1000 and 6000
85 m a.s.l. (Bonadonna et al., 2022; Milford et al., 2023; Hedelt et al., 2025) and were transported over North
86 Africa and Europe, as well as across the Atlantic to the Caribbean on several occasions (Hedelt et al., 2025).
87 Total SO₂ emissions were estimated to be about 1.84 Mt (Milford et al., 2023) using the daily mass estimates
88 derived from the TROPOspheric Monitoring Instrument (TROPOMI) measurements and provided by
89 MOUNTS-Project ([mounts](#), Valade et al., 2019).

90 Geophysical and geochemical co-eruptive observations revealed insights into the structure of the
91 plumbing system (d'Auria et al., 2022; Dayton et al. 2023) and melt evolution during the eruption (Day et al.,
92 2022; Ubide et al., 2023; Dayton et al., 2024; Longpré et al., 2025). Co-eruptive shallow and deep seismicity
93 were recorded, the first one ranging between 5 and 15 km depth starting on 26 September 2021 and remaining
94 until the end of the eruptive period, and the second one ranging between 20 and 25 km depth occurring from 1



October to 13 December 2021 (d'Auria et al., 2022). Additionally, a temporal progression in the melt chemical composition was observed: the initial erupted magma exhibited a tephritic composition (MgO ~6 wt% and TiO₂ ~4 wt%) and was gradually (< day 20; Day et al. 2022) replaced with a basanitic magma (MgO ~8 wt% and TiO₂ 3.7 wt%) for the rest of the eruption (Day et al., 2022; Ubide et al., 2023). This type of transition reflects a behaviour similar to that previously documented for the 1949 and 1971 Cumbre Vieja eruptions (Klügel et al., 2000), and was interpreted as mixing between a resident mush and deep fresh basaltic magmas in the shallow reservoir. Such changes in magma composition could contribute to changes in eruptive dynamism and could be reflected in surface gas composition changes. In fact, variability in the eruptive dynamism was observed through seismic and deformation monitoring, tephra analysis and geochemical lava and ash studies (Bonadonna et al., 2022; 2023; Birnbaum et al., 2023 and references therein). In the early phase of the Tajogaite eruption, rapid cone growth and vent openings were accompanied by explosive tephra ejections. On 25 September, a significant cone collapse was accompanied by increasing explosive activity with evidence of white xeno-pumice fragments in tephra (Day et al., 2022; Romero et al., 2022). Lava evolved from a'a' to fluid basaltic flows with changing composition. By late October-November, plume height stabilized at 2500–3500 m a.s.l. (Córdoba-Jabonero et al., 2023), with lower SO₂ emissions (Milford et al., 2023). The final weeks saw intense activity, collapses, structural changes and vents reconfiguration (Gonzalez, 2022; Walter et al., 2023).

To date, only a few studies have reported the composition of the gas plume measured during the Tajogaite eruption, and none have provided a multi-species time series of estimated emission fluxes over the entire eruptive period. Ericksen et al. (2024) derived CO₂ volcanic emission fluxes from drone-borne SBA-5 infrared CO₂ sensors measurements and also measured CO₂/SO₂ ratios using ground-based Multi-GAS instruments localized near the vent. Burton et al. (2023) reported the first time series of the CO₂/SO₂ ratio of the Tajogaite plume, employing ground-based FTIR spectrometry techniques using incandescent ash plumes, lava fountaining and lava flow as thermal sources, and occasional solar absorption measurements. They also reported drone-borne and ground-based MultiGAS in-plume measurements. Recently, Asensio-Ramos et al. (2025) reported the first time series of CO₂/SO₂, SO₂/HCl and CO/CO₂ ratios measured at the base of the eruptive column using open-path FTIR measurements with lava fountaining and lava flows as thermal source. Using the surface gas measurements, petrological data and estimates of lava emission rates, these authors reveal evidence of exceptional CO₂-rich gas emission with respect to the emitted lava volume during the eruption. Recent studies showed the presence of particularly SO₂- and CO₂-rich compositions of deeply entrapped-MI in volcanic rocks from the Canary Islands (Longpré et al., 2017; Taracsak et al., 2019), which may be linked to mantle metasomatism (Hansteen et al., 1991; 1998).

In this study, we present a comprehensive time series from 21 September 2021 to the end of the eruption of CO₂, CO, HCl, HF to SO₂ ratios measured in the Tajogaite volcanic plume at distances up to 140 km, using ground-based direct-sun FTIR and DOAS instruments that are part of global atmospheric observation networks. Ground-based FTIR and UV direct-sun methods provide multi-species and time-resolved total column measurements of the main volcanic gases, regardless of the plume altitude, while ensuring operators and instruments safety (Butz et al., 2017; Taquet et al., 2023). They have the advantage of using the sun as a common and both homogeneous and constant-intensity source (at the timescale of a single measurement), providing solar spectra in a wide spectral range and with a high signal-to-noise ratio. We also took advantage of the instrumental suite installed at the Izaña Atmospheric Observatory (IZO) in Tenerife. Its high altitude and geographical location were ideal for repeatedly directly capturing the volcanic plume including with surface measurements, thereby enhancing the temporal density of our dataset. We estimated daily SO₂ volcanic emission fluxes from space-based TROPOMI/Sentinel-5P measurements, and used the measured species-to-SO₂ ratio to derive the emission fluxes of the other volcanic species and their total emissions. Our results are interpreted in the light of petrological (including new melt inclusions and matrix glass compositions) and geophysical data.

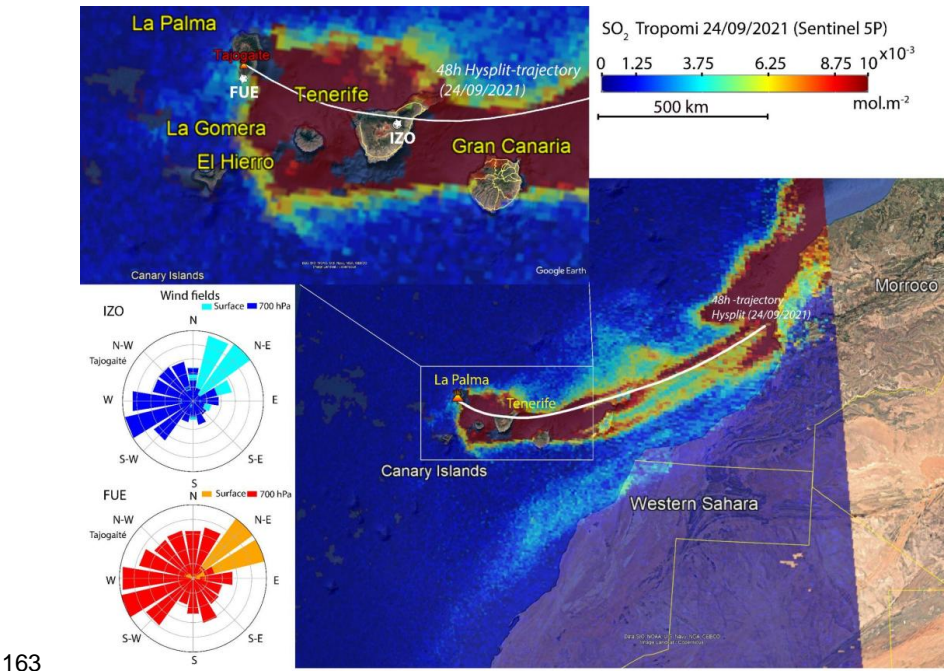
2. Measurement sites and instrumentation

A comprehensive network for the monitoring of trace gases, aerosols and ash fallout was operative for air quality monitoring and scientific research during the eruption. Monitoring efforts relied on a combination of



144 permanent stations which are part of international atmospheric research and air quality monitoring networks,
145 such as those in the Canary Islands Government Air Quality Monitoring Network (AQMN) and the facilities at
146 IZO, as well as additional infrastructures specifically installed for attending the volcanic emergency. In this
147 framework, the State Meteorological Agency of Spain (AEMET), through Izaña Atmospheric Research Center
148 (IARC) and the Territorial Delegation of AEMET in the Canary Islands (DTCAN) and in collaboration with the
149 Spanish National Research Council (CSIC) and other institutions, deployed scientific instrumentation on La
150 Palma. The objectives of the deployment were: 1) real-time monitoring and characterization of the vertical
151 structure of the eruptive plume, carried out through the implementation of an aerosol profiling network in the
152 context of the European Aerosol, Clouds and Trace Gases Research Infrastructure (ACTRIS, 2021; Barreto et
153 al., 2022; Álvarez et al., 2023); 2) complementing the air quality network observations managed by the
154 Government of the Canary Islands (Milford et al., 2023, and references therein); and 3) investigating the
155 physicochemical composition of the volcanic plume, its links with the evolution of the eruptive process and
156 studying the ash-gas-aerosol interactions (Garcia et al., 2022; Cordoba-Jabonero et al. 2023; Cuevas et al., 2024,
157 and references therein).

158 We conducted specific columnar and in-situ gas and ash measurements during the entire eruptive
159 period at two stations localised in La Palma (FUE) and Tenerife (IZO) islands (Fig. 1) to assess the co- and post-
160 eruptive compositional variability of the Tajogaite volcanic plume. Figure 1 displays a mapping of the two
161 stations concurrently with a typical SO₂ plume as detected by space-based TROPOMI/Sentinel-5P sensor. The
162 instruments at each site and the measurement periods are summarised in Table 1 and detailed below.



163
164 **Figure 1: Location of our measurement stations in Canary Islands during the 2021 La Palma eruption (FUE and IZO**
165 **represent the Fuencaliente and Izaña stations, respectively, marked by white stars). SO₂ data from**
166 **TROPOMI/Sentinel-5P sensor are shown in the map for 24 September 2021, illustrating the typical plume dispersion**
167 **over hundreds of kilometres. The instruments implemented at FUE and IZO stations are summarised in Table 1.**
168 **Wind rose diagrams for surface and 700 hPa levels (corresponding to the average of the plume altitude during the**
169 **eruption) are also presented for the IZO and FUE stations, considering the entire eruptive period and the ECMWF**
170 **Reanalysis v5 (ERA5) data (ECMWF: <https://www.ecmwf.int/en/forecasts/dataset/ecmwf-reanalysis-v5>).** Base map
171 **was obtained from © Google Earth (©Google).**



Table 1: Solar FTIR and surface in situ measurements conducted at the FUE and IZO stations from 21/09/2021 to 21/01/2022.

Station (Island) (geographical coordinates) altitude distance from the eruptive fissure	Instrument (Networks)	Measurement period	Fraction of measurement days capturing the volcanic plume
FUE (La Palma) (28.49°N, 17.85°W) 630 m a.s.l. ~ 15 km	EM27/SUN#SN143 (COCCON)	25/09/2021 - 21/01/2022	21/59 (co-eruptive) 1/11 (post-eruptive)
	Combined EM27/SUN#SN143- DOAS	10/10/2021 - 10/12/2021	14/32 (co-eruptive)
IZO (Tenerife) (28.31°N, 16.50°W) 2370 m a.s.l. ~ 140 km	EM27/SUN#SN085 (COCCON)	20/09/2021 - 31/01/2022	4/38 (co-eruptive) 0/9 (post-eruptive)
	IFS-125HR (NDACC)	19/09/2021- 31/01/2022	11/48 (co-eruptive) 0/13 (post eruptive)
	In situ UV fluorescence analysers (SO ₂) (GAW WMO network)	21/09/2021- 31/12/2021	26/83 (co-eruptive) 1/16 (post eruptive)
	In situ Picarro (CO ₂ , CO) (GAW WMO network)	19/09/2021- 31/12/2021	26/85 (co-eruptive) 1/16 (post eruptive)

2.1. The Fuencaliente (FUE) station (La Palma island)

In the context of AEMET responsibilities, as a State Agency, for continuous monitoring of the meteorological and climatic conditions and of atmospheric composition, a specific instrumental deployment has been set up in La Palma. In particular, a new station for gas and particle monitoring was implemented at the San Antonio Volcano visitors center of Fuencaliente, at the southern tip of La Palma island, ~15 km from the eruptive fissure of the Tajogaite volcano (Fig. 1). The FUE station included a wide range of instruments such as a sun-lunar Cimel CE318T photometer, contributing to the Aerosol Robotic Network (AERONET), for aerosol column measurements, a Lufft CHM15k ceilometer for aerosol and cloud vertical profiling and an all-sky camera for weather monitoring (Román et al., 2021) and a tephra trap.

A few days after the beginning of the eruption (on 25 September 2021), we deployed an EM27/SUN spectrometer (developed by Karlsruhe Institute of Technology, in collaboration with Bruker Optics, Germany), which is the standard instrument of the Collaborative Carbon Column Observing Network (COCCON, Frey et al., 2019) dedicated to the measurement of greenhouse gases. This portable Fourier Transform Infrared (FTIR) spectrometer, equipped with a Quartz beamsplitter and two InGaAs photodetectors, provides low-spectral resolution (0.5 cm^{-1}) solar absorption spectra in the Near-Infrared (NIR) range (from 4000 to 11000 cm^{-1}), allowing the analysis of COCCON standard species (CO₂, CO, H₂O, CH₄). It records double-sided forward-backward interferograms with a scanner velocity of 10 kHz and typically averages ten scans, so that a spectrum is acquired approximately every minute. The spectral range of this instrument also allows for obtaining other gas species of interest for volcanology and air quality studies, such as halogen halides (HCl, HF) (Butz et al., 2017). From 10 October 2021 to 10 December 2021, following Butz et al. (2017) approach, we combined the EM27/SUN with a UV-Vis DOAS spectrometer (model Avantes ULS2048), recording spectra in the 270-425 nm spectral range with a spectral resolution of 0.4 nm. Both instruments shared the incident sun radiation from the EM27/SUN solar tracker to add simultaneous measurements of SO₂ and BrO with the same measurement configuration (Fig. 2).

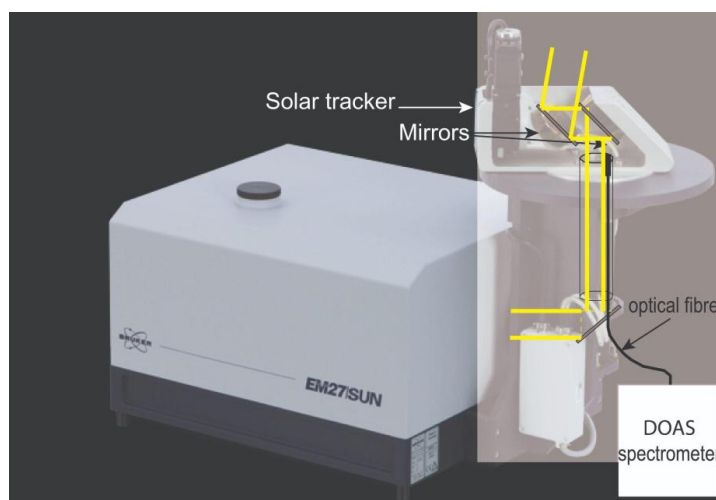


Figure 2: Schematic set-up of the combined EM27/SUN-DOAS direct-sun measurements implemented at the FUE station during the Tajogaite eruption (La Palma island). The DOAS optical fibre is introduced and attached in the FTIR sunlight collection tube, pointing towards the solar tracker mirrors. The yellow lines schematize the incident sunlight optical path. Original photo was obtained from Bruker website (<https://www.bruker.com/>).

The DOAS fibre was inserted and attached coaxially into the tube directing the light from the solar tracker toward the EM27/SUN spectrometer entrance (Fig. 2). By this way, it allows collecting the maximum light intensity with a minimal disturbance of the solar beam transmitted to the EM27/SUN. The fibre was connected to the DOAS spectrometer, installed in a protective case sheltered from solar radiation near the EM27/SUN instrument. DOAS direct-sun absorption spectra were routinely recorded using the MobileDOAS software provided by the IASB/BIRA Institute with an integration time of about 30 seconds.

2.2. The Izaña Atmospheric Observatory (IZO, Tenerife island)

The proximity of the island of Tenerife to La Palma and the location of the IZO station in the free troposphere resulted in it being affected several times by the Tajogaite volcanic plume. This allowed for a more in-depth study of various aspects of the volcanic eruption from a multi-instrumental perspective. Indeed, given its strategic location and its excellent atmospheric conditions, IZO has a comprehensive programme for atmospheric composition measurements. Uninterrupted meteorological and climatological observations started in 1916 and, since 1984, IZO has contributed to the GAW-WMO (Global Atmosphere Watch, World Meteorological Organization) programme and to multiple international networks and databases (WDCGG, WUOUC, NDACC, TCCON, COCCON, AERONET, BSRN, MPLNET, E-GVAP, NOAA/ESRL/GMD CCGG, etc.; Cuevas et al., 2024, and references therein). Within IZO's atmospheric research activities, the station is equipped with a high-resolution IFS-125HR and low-resolution EM27/SUN FTIR spectrometers, which provide long-term solar absorption measurements from 1999 and 2018, respectively. The EM27/SUN spectrometer is the same model instrument as that implemented at the FUE station allowing the analysis of CO₂, CO, HF and HCl species and previously described.

The IZO FTIR spectrometers routinely contribute to the Network for the Detection of Atmospheric Composition Change (NDACC, <https://ndacc.larc.nasa.gov>, last access: March 2025), Total Carbon Column Observing Network (TCCON, <https://tcon-wiki.caltech.edu>, last access: March 2025), and COCCON (<https://www.imk-asf.kit.edu/english/COCCON.php>, last access: March 2025) (Schneider et al., 2005; García et al., 2021). As part of NDACC activities, direct solar mid-infrared (MIR) absorption spectra are measured in the range of 700 to 4500 cm⁻¹, with a spectral resolution of 0.005 cm⁻¹. NDACC operations involve co-adding several scans to increase the signal-to-noise ratio, resulting in each spectrum acquisition taking several minutes. García et al. (2021) provide further details about the IZO FTIR program. The IZO IFS-125HR MIR solar spectra were used to analyse the SO₂ species alongside HCl and HF, which were also measured from the EM27/SUN



spectra (unlike SO_2). This approach further allowed us to evaluate the uncertainties associated with our new retrieval methods for the HF and HCl species (see section 3 and Appendix A).

Moreover, as part of the GAW-WMO programme, continuous surface measurements of CO_2 (since 1984), SO_2 (since 2006), and CO (since 2008) are performed at IZO. Different in situ analysers and measurement techniques have been used for measuring these gases: CO_2 with non-dispersive infrared (NDIR) gas Licor analysers, CO with gas chromatography (GC) Trace Analytical RGA-3 instruments and SO_2 with ultraviolet (UV) fluorescence analysers (Thermo 43C-Trace Level). Since 2015, CO_2 and CO have also been monitored using a cavity ringdown spectroscopy (CRDS)-based Picarro G2401 instrument. These observations are carried out following the strict GAW-WMO measurement protocols and their quality is periodically assessed by external audits by the World Calibration Centre for surface Ozone, CO, Methane and CO_2 (WCC-Empa). The bias for the CO_2 and CO measurements in the frame of the GAW-WMO network is ± 0.1 ppm and ± 2 ppb, respectively (WMO, 2018). For SO_2 , the uncertainties are expected to be around ± 0.2 ppb (manufacturer specifications; see also Cuevas et al., 2024 and references therein). This continuous gas monitoring captured the Tajogaite plume composition on several occasions, when meteorological conditions allowed rapid and direct transport to the IZO station.

2.3 Mobile MultiGAS

During the eruptive period, surface MultiGAS measurements (SO_2 , CO_2 , H_2O , H_2S) were carried out into the volcanic plume, between 28 September and 10 October 2021, when meteorological conditions allowed it to be sampled at ground level at a high concentration. The instrument consists in a MSR145 datalogger connected to an Edinburgh Gascard NG with a pump measuring as a CO_2 sensor, measuring in the range 0-1000 ppm, a City Technology T3ST/F electro-chemical SO_2 sensor measuring in the range 0-50 ppm and a City Technology T3H electro-chemical H_2S sensor measuring in the 0-20 ppm range. SO_2 concentrations up to 7 ppm were measured at distances of about 2 km East and West of the vent. Time series of concentrations of the different gas species were correlated by adjusting the time-lag and smoothing parameter until the best R-squared correlation coefficient was obtained. The measurements presented here have R-squared better than 0.75.

3. Gas retrievals and particulate matter complementary analyses

3.1. Gas analysis from direct-sun spectroscopic absorption spectra

3.1.1. EM27/SUN spectral analysis (CO_2 , CO, HCl and HF)

The processing of EM27/SUN measurements was performed using the open-source PROFFAST pyotv1.2 packages developed by KIT and used by the COCCON community. The COCCON standard retrieval procedure used for the analysis of atmospheric CO_2 , CO, CH_4 and H_2O species is fully described in Frey et al. (2019), Alberti et al. (2022), Herkommer (2024a,b) and Feld et al. (2024). Here, we provide details only on the specific retrieval strategies that we developed for volcanological applications. The PROFFAST package includes a preprocess code generating the required spectra by a Fast Fourier Transform. The processing incorporates various quality checks, as a signal threshold, intensity variations during recording, requirement of proper spectral abscissa scaling, and generates spectra only from raw measurements passing all checks (the remaining ones being flagged). We used the Instrumental Line Shape (ILS) parameters reported in Alberti et al. (2022) following the COCCON standard recommendations. Calibrated spectra are then analysed using the PROFFAST radiative transfer and inversion models to derive the total columns by scaling the a priori Volume Mixing Ratio (VMR) profiles iteratively until adjusting the simulated spectra to the measured spectra. Surface pressures are derived from the in situ high precision sensor measurements (PCE-THB-40 at FUE and SETRA-470 at IZO). All the EM27/SUN retrievals presented in this study were performed using the 2020 HITRAN spectroscopic line lists (Gordon et al., 2022). We used meteorological data and a priori VMR profiles based on the sub-daily available GGG2020 TCCON meteorological data (MAP files downloaded from the Caltech server and based on National Centers for Environmental Prediction (NCEP) reanalysis). We adapted the a priori VMR profiles for the target species depending on whether the gas is purely volcanic (low atmospheric abundance) or also has an atmospheric background. The spectral windows and retrieval strategies used for each species are presented in Table 2 and detailed below.



281 For the analysis of HCl and HF species, we utilized a priori VMR profiles with high concentrations
282 (1×10^{-4} ppm) up to the altitude of the volcanic plume (~6 km a.s.l., based on IGN/AEMET; Milford et al.,
283 2023), and VMR concentrations for the upper levels derived from the Whole Atmosphere Community Climate
284 Model (WACCM v.6, <https://www2.aom.ucar.edu/gcm/wacm>, last access: february 2025) average profiles
285 provided by the National Center for Atmospheric Research (NCAR; James Hannigan, personal communication,
286 2014), which are commonly used by the NDACC community. In this case, we adapted the PROFFAST retrieval
287 inputs so that only the tropospheric portion (up to the altitude of the volcanic plume) was scaled, keeping the
288 stratospheric part as constant. This approach was previously employed to measure volcanic emissions of HCl
289 and HF from Mt. Etna, also relying on low-resolution EM27/SUN spectra (Butz et al., 2017), but utilizing the
290 PROFFIT package for the retrieval. We used new optimised spectral windows (Table 2, HCl_v2 and HF_v2) for
291 the analysis of these two species to be able to even detect very low concentrations, as well as that detected at the
292 IZO station, 140 km from the eruptive fissure. The analysis was also conducted using the same spectral ranges
293 as Butz et al. (2017) (HCl_v1 and HF_v1 in Table 2) to evaluate the consistency and improvements introduced
294 by the new strategies for our application. Appendix A gives a full comparison between the results obtained
295 using the new and Butz et al. (2017) retrievals, as well as with those from the high-resolution spectra analysis
296 (see section 3.1.3) for side-by-side measurements.

297 For the retrieval of volcanic CO and CO₂, due to their high atmospheric abundance and variability, we
298 used the COCCON standard retrievals (scaling of the whole profile and use of the COCCON spectral windows
299 and TCCON priori VMRs) and then removed the atmospheric background to derive the volcanic contribution.
300 The column-averaged dry-air mole fraction of CO₂ and CO (XCO₂ and XCO) were estimated using the O₂ total
301 columns according to Wunch et al. (2011) ($X_{gas} = 0.2095 \times V_{gas} \div VO_2$) after applying air mass independent
302 and dependent correction factors (AICF and ADCF). We have slightly modified the standard procedure for
303 performing the O₂ retrieval by adding HF as species to be retrieved, using a specific a priori VMR profile based
304 on the WACCM v.6 climatology. However, the HF profile was adjusted to have a constant and significantly
305 higher concentration (1×10^{-4} ppm) up to the maximum plume altitude. For the other interfering gases, we used
306 the a priori VMRs derived from the TCCON GGG2020 MAP files.

307 To remove the background atmospheric concentrations of XCO₂ and XCO, we used the daily-averaged
308 IZO X_{gas} time series to model the long-term natural variability with a third-degree polynomial, which was then
309 interpolated and subtracted from the FUE XCO₂ and XCO time series. For CO₂, an additional intraday
310 variability had to be taken into account. It was simulated by averaging and fitting some intraday IZO XCO₂ time
311 series which were not affected by the volcanic plume. Intraday simulations were performed for each day, using
312 the average fit and adjusting the offset. Examples of background fits are given in Fig. A3. The accuracy of the
313 method was assessed by comparing the simulated XCO₂ background at the station impacted by the volcanic
314 plume with the measured XCO₂ background at the other station when it was not affected by the plume (Fig. A3).
315 The average and maximum absolute difference arising from this procedure were found to be 0.1 and 0.8 ppm in
316 extreme cases. Finally, the ΔCO_2 and ΔCO total columns corresponding to the volcanic enhancements were
317 determined from the X_{gas} enhancements by multiplying them by the dry air columns derived from the surface
318 pressure measurements and H₂O total columns (Wunch et al., 2011).

319 **Table2: Retrieval parameters used for the EM27/SUN spectral analysis. “Sim” corresponds to the interfering species**
320 **only considered for the forward simulations. “*” refers to similar spectral windows as Butz et al. (2017).**

Gas	Spectral Window (cm ⁻¹)	Interfering Gases	Strategy
HCl_v1 HCl_v2	5684.0 - 5795.0* 5703.5 - 5779.0	H ₂ O, HDO, CH ₄ H ₂ O, HDO, CH ₄	High (1×10^{-4} ppm) a priori HCl VMR between 0 - 5.8 km beyond: WACCM v.6
HF_v1 HF_v2	7765.0 - 8005.0* 3995.0 - 4043.0	H ₂ O, CO ₂ (Sim), O ₂ H ₂ O, HDO, CH ₄	High (1×10^{-4} ppm) a priori HF VMR between 0 - 5.8 km beyond: WACCM v.6
CO ₂	6173.0 - 6390.0	H ₂ O, CH ₄ (Sim)	COCCON + post-process background correction



CO	4208.7 - 4318.8	H ₂ O, HDO, CH ₄ , N ₂ O (Sim), HF (Sim)	COCCON + post-process background correction
O ₂	7765.0 - 8005.0	H ₂ O, CO ₂ (Sim), HF	High (1×10^{-4} ppm) a priori HF VRM between 0 - 5.8 km beyond: WACCM v.6

3.1.2 DOAS analysis (SO₂)

Solar DOAS spectra were processed using the QDOAS v2.111 software (Dankaert et al., 2014), applying a Levenberg-Marquardt (LM) algorithm to retrieve the Slant Column Densities. We used the same analysis strategy as described in Taquet et al. (2023). Wavelength calibration and slit function were determined by laboratory close-path measurement using a low-density mercury lamp, and further adjusted based on the position and widening of the Fraunhofer lines during the QDOAS processing. SO₂ was retrieved in the 312.0–326.8 nm spectral window according to Butz et al. (2017). The high resolution solar spectrum from Chance and Kurucz (2010) was used as the reference spectrum. We used the cross-section at 298 K from Vandaele et al. (2009) for SO₂ and the cross-section at 221 K from Burrows et al. (1999) for the interfering gas O₃. A third-order polynomial function was included in the fitting routine to remove the broadband extinction. The I0 effect, due to the limited resolution of the spectrometers (Platt et Stutz, 2008), was corrected using the QDOAS I0-correction algorithm applied for six fixed SO₂ slant column values of 0.0, 1.0×10^{18} , 2.0×10^{18} , 3.0×10^{18} , 4.0×10^{18} , 5.0×10^{18} molec/cm² (the latter is close to the maximum uncorrected slant column). Then, each corrected value is determined by interpolating the corrected slant columns values. Finally, SO₂ slant columns were converted into vertical columns by dividing them by the SZA-dependent air mass factor ($1/\cos(\text{SZA})$) to be combined with the FTIR data. An analysis of BrO was also performed using the same parameters as described in Taquet et al. (2023), but this compound was not detected during the measurement period.

3.1.3. IFS-125HR analysis (HCl, HF and SO₂)

The HCl and HF retrieval strategy from the IFS-125HR spectra is based on the NDACC-IRWG recommendations (Infrared Working Group, IRWG, 2014), and on the adapted retrievals for volcanological applications reported in Taquet et al. (2019) and Stremme et al. (2023). However, they have been optimised here to properly capture tropospheric volcanic contributions up to 140 km from the eruptive fissure. Consistently with the NDACC approach, both species were retrieved using the non-linear least-squares fitting algorithm PROFFIT (Profile Fit, Hase et al., 2004), and considering the specified spectral regions and interfering gases given in Table 3. The inversion procedure is solved using a first-order Tikhonov–Phillips regularization (L1, Rodgers, 2000) on a logarithmic scale, where the VMR a priori profiles for the interfering gases are taken from WACCM v.6 climatological profiles. The NCEP 12:00 UTC daily temperature and pressure profiles are employed for the radiative transfer simulations.

The most significant changes with respect to NDACC involved the a priori VMR profiles considered for the target gases, vertical L1 regularization, and the spectroscopic database. Similarly to the EM27/SUN analysis, we adopt modified HF and HCl a priori VMR profiles with high concentrations (1×10^{-4} ppm) up to the maximum plume altitude (~6 km a.s.l.), which are completed for the IFS-125HR using WACCMv.6 information beyond this altitude. In addition, the 2020 HITRAN spectroscopic linelists were utilised for all gases. Finally, in contrast to the NDACC approach, where the lowermost and uppermost altitude levels are fixed to the a priori to ensure stability in the retrieval, in this study, the first level is left unconstrained to provide flexibility in the retrieval process in the lower troposphere.

In the case of SO₂, a harmonized and standardized FTIR strategy is not available within NDACC. Therefore, in this work, we employ the strategy developed by García et al. (2022), which has been successfully applied to various NDACC FTIR sites affected by volcanic SO₂ emissions (Smale et al., 2023; García et al., 2025). This approach is based on the study by Taquet et al. (2019), which presents SO₂ total column amounts from the measured solar absorption spectra in the 2500 cm⁻¹ region using a scaling retrieval and the inversion code PROFFIT. Similarly to HF and HCl volcanic products, the SO₂ a priori VMR profiles are adapted in the lower troposphere, while climatological WACCMv.6 profiles are considered for all interfering gases (Table 3).



Appendix A provides a summary of the comparison between the standard NDACC HCl and HF products and those developed in this study, the new IFS-125HR SO₂ retrievals, as well as the comparison between all the IFS-125HR and EM27/SUN products.

Table 3: Retrieval parameters used for the IFS-125HR analysis. “Sim” corresponds to the interfering species only considered for the forward simulations. The spectral windows are acquired using the NDACC filter SC (S3) for HCl, with the NDACC filter SA (S1) for HF, and with the NDACC filter SF (S6) for SO₂. Therefore, they are almost coincident, but not simultaneous observations.

Gas	Spectral Window (cm ⁻¹)	Interfering Gases	Strategy
HCl	2727.73-2727.83 2775.60-2775.90 2821.40-2821.75 2925.75-2926.10	H ₂ O (Sim), HDO (Sim), O ₃ , CH ₄ (Sim), OCS, NO ₂ , N ₂ O (Sim)	High (1×10 ⁻⁴ ppm) HCl a priori VMR between 0 - 5.6 km, above: WACCM v.6
HF	4000.90-4001.05 4038.85-4039.08	H ₂ O, O ₃ (Sim), CH ₄ (Sim)	High HF (1×10 ⁻⁴ ppm) a priori VMR between 0 - 5.6 km, above: WACCM v.6
SO ₂	2480.00-2520.00	H ₂ O, CO ₂ , O ₃ , CH ₄ , N ₂ O	High SO ₂ (1×10 ⁻² ppm) a priori VMR between 0 - 5.6 km, above: WACCM v.6

3.2. Retrieval of SO₂ volcanic emission fluxes from TROPOMI data

The SO₂ flux was retrieved by processing the images of the TROPOMI hyperspectral UV-SWIR sensor on-board the Sentinel-5P satellite. The images were processed by the traverse method, initially developed for the coarser TOMS satellite by Bluth et al. (1994) and later adapted to more recent sensors such as OMI and TROPOMI. The traverses are drawn across the plume semi automatically and the SO₂ flux is calculated using the equation:

$$F = \sum Xi * Li * \sin(\theta) * v$$

where Xi is the SO₂ Vertical Column Density (VCD), L is the length of the pixel, θ is the angle between the pixel row and the wind direction, and v is the plume transport speed. The SO₂ VCD was interpolated at plume height between the SO₂_1km and the SO₂_7km subproducts of the version 3 of the TROPOMI SO₂ product, described in Theys et al. (2021). The plume speed was obtained from the Global Data Assimilation System model of the NOAA, through the READY Archived Meteorology portal (<https://www.ready.noaa.gov/index.php>). For the flux calculation, we used the average wind speed at the plume altitude over the analysed plume portion. The traverse method does not work in cases of plume stagnation in a low wind environment and when the plume is split into several directions due wind shear. These situations happened during about 30% of the time of the eruption, causing some gaps in the SO₂ flux time series.

3.3. Determination of sulphate aerosol

Samples of aerosols, or particulate matter (PM), smaller than 10 μm (PM₁₀) were collected at two sites in La Palma, at El Paso and at Los Llanos de Aridane. In Tenerife island, the samples were collected in Izaña Atmospheric Observatory. We used high volume samplers (30 m³.h⁻¹) and quartz microfiber filters (150 mm diameter). Sulphate concentrations were determined by ion chromatography (Metrohm™ 930 Compact IC FLEX), after an leaching extraction in deionized milli-Q grade water of the sample by methods described in Rodríguez et al. (2012).

3.4. Volcanic glass S, Cl and F contents and sulfide droplet composition

We report new compositions of MIs hosted in olivine, clinopyroxenes and amphibole (kaersutite) crystals. We also report Cl, F and S contents in tephra glasses that were measured during the analyses published in Gonzalez-Garcia et al. (2023). The volatiles were analysed using a Cameca SX-100 electron microprobe



(EPMA) at the Department of Geosciences of the University of Bremen (Germany), with an acceleration voltage of 15 kV, beam current of 40 nA and defocused beam of 10 μm , following the methods described in Gonzalez-Garcia et al. (2023). The instrument was calibrated with a natural fluorite for F, pyrite for S, and Smithsonian scapolite for Cl. Counting times on peak were 120 s for F and 60 s for S and Cl. The analyses of F used the PHA (pulse height analysis) setting after Zhang et al. (2016); the interference of the $\text{FeL}\alpha$ line on the $\text{FK}\alpha$ peak was corrected using the overlay function of the Cameca software. The Smithsonian reference materials VG-2 glass, VG-A99 glass and Kakanui hornblende (Jarosewich et al., 1980) were analyzed along with the samples for precision and accuracy control. Accuracy is better than 6% for S and Cl and >20% for F; reproducibility is typically better than 10%. In addition, the composition of two sulfide droplets was semiquantitatively estimated by EDX (energy-dispersive X-ray) spectroscopy.

A Scanning Electron Microscope (SEM) was used to obtain high-resolution back-scattered electron (BSE) images of two sulfide droplets found in the tephra sample LM-2309 (Las Manchas, 23 September). The BSE images were acquired using a JEOL JSM-7610F gun emission scanning electron microscope installed at the Institute of Earth System Sciences, Leibniz Universität Hannover, Germany, using an accelerating voltage of 15kV and a working distance of 15 mm. Bruker ESPRIT software was used for image acquisition.

4. Results

4.1. Evolution of the volcanic plume composition during the Tajogaite eruption

The temporal variability of the Tajogaite plume composition is examined through the time series of the ratios, some of them involving species with contrasting exsolution depths. Daily CO_2/SO_2 , HCl/SO_2 , HF/SO_2 , HCl/CO_2 , HF/CO_2 , CO/SO_2 and CO/CO_2 molecular ratios were estimated from the daily correlation plots of the total column time series (using a similar methodology as detailed in Taquet et al., 2019, 2023) and are reported in Fig. 3. The same method used for column-averaged ratios was applied to calculate the surface concentration ratios from GAW and multiGAS measurements (also presented in Fig. 3). The background contribution of atmospheric species (CO_2 and CO) to these measurements was removed using daily polynomial curves fitted from the surface measurements without contribution of volcanic emissions (i.e. $\text{SO}_2 < 0.05$ ppm). Additionally, we reported in the same Figure our multiGAS CO_2/SO_2 measurements, obtained on 29 September, 2 and 7 October from Las Manchas (~500 m a.s.l., SW from the eruptive fissure) and from the El Jable viewpoint (2100 m a.s.l., E of the eruptive fissure), ranging between 1.7 and 14.3. Figure 3 also includes the columnar and surface measurements reported in the literature (Burton et al., 2023; Eriksen et al., 2024). The scarcity of FTIR measurements from early November until the end of the eruption, across all measurement techniques, is mainly due to poor or unsuitable weather conditions.

Our CO_2/SO_2 column-averaged molecular ratios range between 9 ± 6 and 63 ± 28 ($9\text{--}24$ at IZO and $14\text{--}63$ at FUE) during the eruption and are consistent with the ratios derived from the IZO surface data (from 5.6 ± 0.1 to 18.3 ± 0.7) and from our multiGAS measurements at La Palma (1.7 to 14.3). These values are also consistent with those obtained by Burton et al. (2023), ranging between 2 and 52. A remarkably good consistency is observed between the surface and total column measurements at the two sites (FUE and IZO) and the proximal measurements of Burton et al. (2023) and Eriksen et al. (2024). All the measured CO_2/SO_2 ratios define an increasing trend, at least until 2 November 2021 and show more scatter after this date (Fig. 3).

HCl/SO_2 molecular ratios range between 0.02 ± 0.002 and 0.17 ± 0.01 (from 0.02 to 0.05 at IZO and from 0.02 to 0.17 at FUE) and show short-term variations around a nearly constant daily average of (0.05 ± 0.03) throughout the entire eruptive period. These ratios are consistent with the values of SO_2/HCl of 16.8 and 8 ($\text{HCl}/\text{SO}_2 = 0.06$ and 0.12, respectively) reported in Burton et al. (2023), which corresponds to a lava fountaining plume and spattering event. It is also consistent with the more recently published ratios ranging between 0.04 and 0.2 (Asensio-Ramos et al., 2025). HF/SO_2 molecular ratios vary between 0.0012 ± 0.0002 and 0.081 ± 0.007 (from 0.001 ± 0.001 to 0.082 ± 0.007 at FUE and from 0.007 ± 0.002 to 0.037 ± 0.025 at IZO) and show a similar day-to-day variability to that observed for the HCl/SO_2 ratios through the eruptive period. HCl/CO_2 molecular ratios exhibit values from $(6 \pm 1) \times 10^{-4}$ and $(4.1 \pm 0.1) \times 10^{-3}$ at FUE and from $(2 \pm 1) \times 10^{-3}$ to $(3 \pm 1) \times 10^{-3}$ at IZO, while the HF/CO_2 ratios ranges from $(0.5 \pm 0.1) \times 10^{-4}$ to $(4.5 \pm 0.1) \times 10^{-3}$ at FUE and from $(2.6 \pm 0.3) \times 10^{-4}$ to $(2.7 \pm 0.2) \times 10^{-3}$ at IZO. Like the HCl/SO_2 and HF/SO_2 molecular ratios, HCl/CO_2 and HF/CO_2 exhibit similar day-to-day variability. Their fluctuations include short-term decreasing trends, as observed between 2 and 14 October 2021 and between 21 October and 4 November 2021. The CO/SO_2 FTIR molecular



ratios span from 0.13 ± 0.01 to 0.66 ± 0.03 at FUE and from 0.02 ± 0.01 to 0.17 ± 0.07 at IZO and exhibit an almost constant trend around the average of 0.24 with one extreme event, observed between 1 and 4 November 2021.

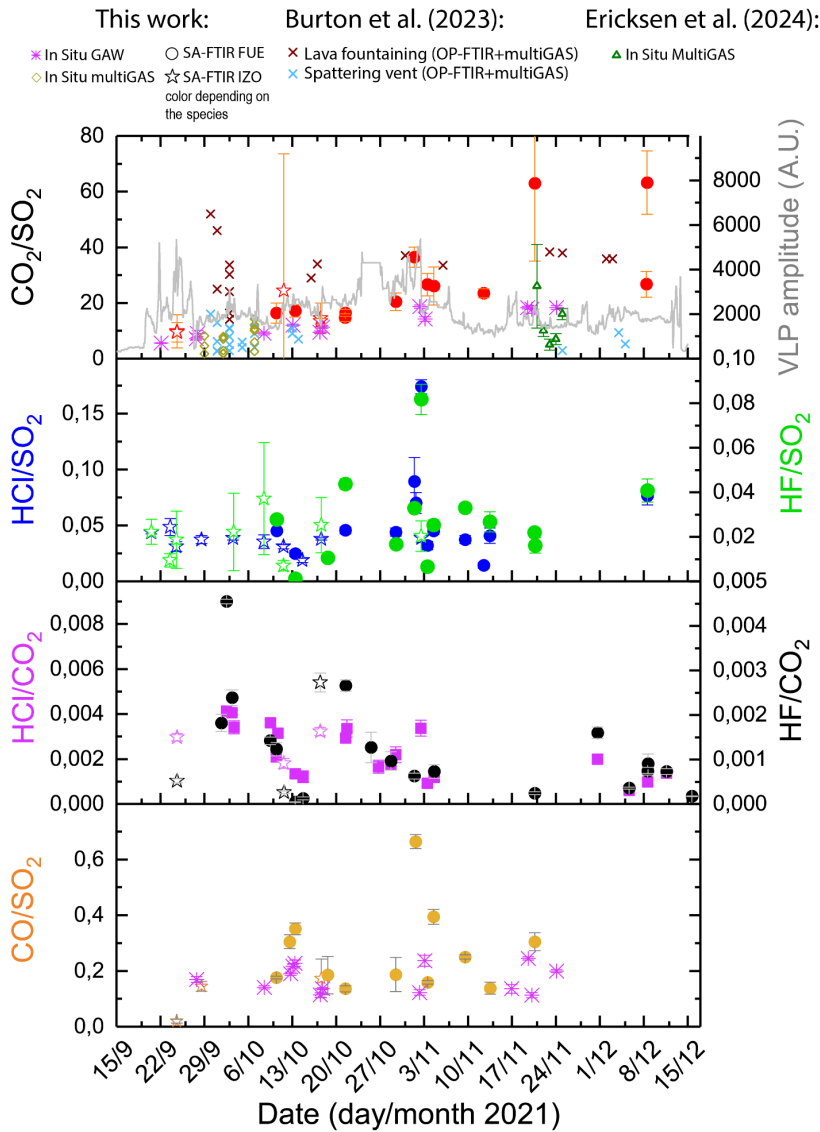


Figure 3: Variability of the Tajogaite volcanic plume composition during the eruption. Daily molecular ratios are calculated from the daily species-to-SO₂ or species-to-CO₂ correlation plots of the total columns (SA: solar absorption FTIR and DOAS measurements) and surface (GAW and multiGAS analysis) time series. Only the ratios with a $R^2 > 0.6$ in the correlation plots are reported here to exclude those with poor reliability. Our CO₂/SO₂ ratios are compared to those reported by Burton et al. (2023) and by Ericksen et al. (2024), where OP corresponds to Open-Path measurements. Very Long Period (VLP; 0.4-0.6Hz) tremor amplitude is taken from Bonadonna et al. (2022).



Our new volcanic plume compositional data for the first days of the eruption, before the 27/09/2021 eruptive pause, is very similar to that of the rest of the eruption, with CO_2/SO_2 values between 5.6 ± 0.1 and 9 ± 1.1 , HCl/SO_2 between 0.031 ± 0.005 and 0.049 ± 0.007 and HF/SO_2 between 0.009 ± 0.003 and 0.022 ± 0.006 . Finally, our time series show a significant and abrupt increase of all species-to- SO_2 ratios on 2-3 November 2021, which also coincides with a minor peak in the HCl and HF -to- CO_2 ratios. This event represents a notable and enduring change in gas ratio variability involving CO_2 , (i.e. CO_2/SO_2 and HCl/CO_2) and coincides with a sudden decrease in the amplitude of seismic tremor (VLP and LP, Fig. 3 and Bonadonna et al., 2022). Prior to this date, the variability in the CO_2/SO_2 ratio closely followed the increasing trend of VLP tremor amplitude, while afterwards it declined and exhibited a noticeable short-term variability until the end of the eruption. This noticeable change depicts two periods in our dataset (here after phase I and II), whose relationship with the previously described events and timeframes of the eruption (Bonadonna et al., 2022; Ubide et al., 2023; Milford et al., 2023) will be discussed in section 5. For HCl/CO_2 and HF/CO_2 , the ratios are significantly lower during phase II (average of 0.0012 ± 0.0005 and 0.0007 ± 0.0004 , respectively) than during phase I (average of 0.0027 ± 0.0009 and 0.0014 ± 0.001 , respectively). For other species, only a sharp increase is noted at this time, but at the beginning of phase II the ratios appear to return to the initial ranges observed during phase I.

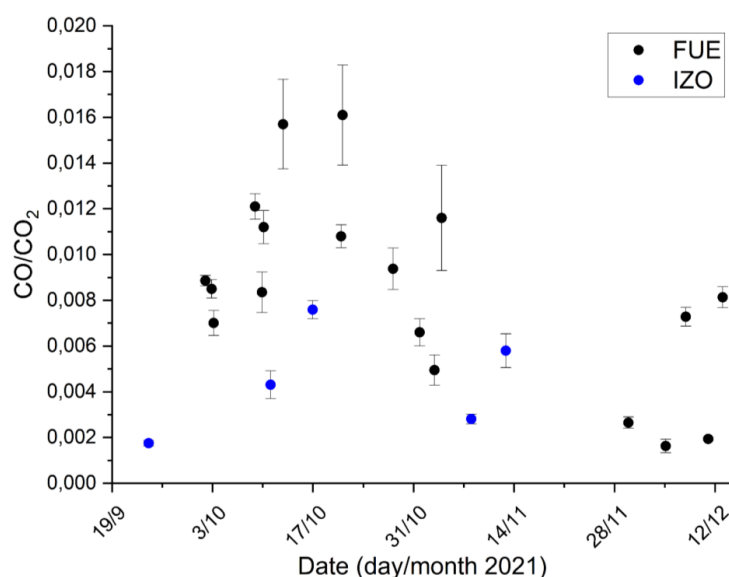


Figure 4: Time series of the CO/CO_2 ratio at both FUE and IZO stations.

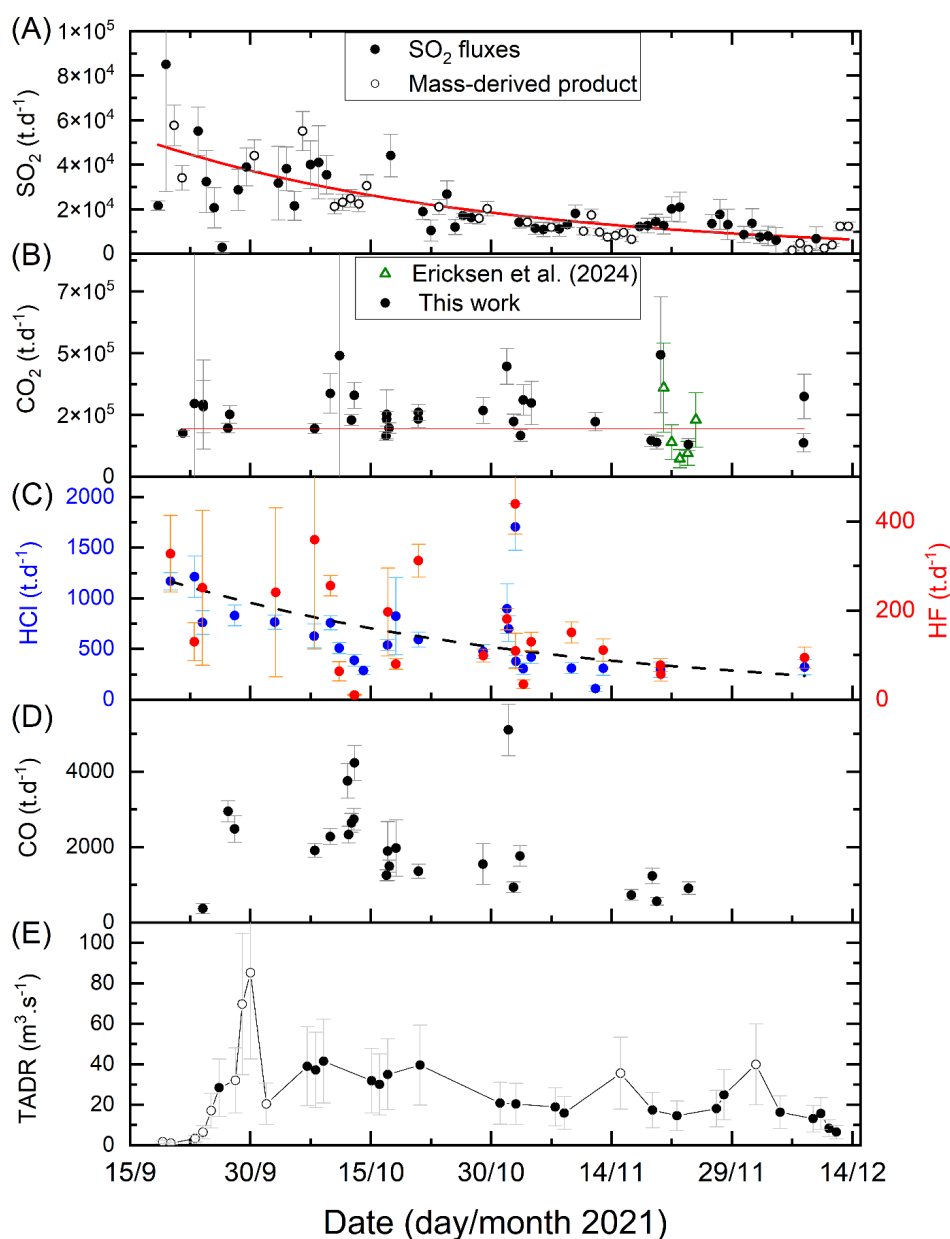
Figure 4 shows the time series of CO/CO_2 derived from the FTIR solar absorption at FUE and IZO stations over the entire eruption. CO/CO_2 time series is very similar at both measurement locations, with a progressive increase from 0.0016 to 0.016 during the first 30 days of the eruption before decreasing again to low values before mid-November. The IZO absolute ratios are consistent with that reported in Álvarez et al. (2023) for this eruption.

4.2. SO_2 , CO_2 and halogen-derived volcanic emission fluxes and total emissions

SO_2 volcanic emission fluxes were estimated whenever the weather conditions made it possible following the method described in section 3.2 and reported in Fig. 5. The SO_2 volcanic emission fluxes retrieved during this eruption exhibited a remarkably strong correlation ($R^2=0.92$, Fig. D3) with the daily SO_2 masses (taken from MOUNTS website; Valade et al., 2019), suggesting that the specific filter applied for ensuring the high quality daily fluxes determinations is likely too restrictive for studying long-term trends. To fill the long-term gaps in our SO_2 fluxes time-series, a less reliable mass-derived product was included, derived from the linear relation between the SO_2 volcanic emission fluxes and daily mass (Fig. 5A, empty circles). This was only applied to



492 days with minimal accumulation. The resulting SO_2 volcanic emission fluxes time series exhibit a decreasing
493 exponential trend, with an equation of the form $y = a \times e^{-bx}$ and a coefficient of determination $R^2 = 0.63$.



494
495 **Figure 5: (A) to (D) Emission fluxes of SO_2 , CO_2 , HCl, HF and CO and (E) corrected TADR, following Plank et al.**
496 **(2023), during the eruption. The thick red line in (A) is the exponential fit to the SO_2 emission fluxes time series. The**
497 **red line in (B) is the linear regression for the dataset. The black dashed line in (C) is the exponential fit to the HCl**
498 **time series. Black points in (E) are part of the TADR- SO_2 emission flux correlation.**

499 Volcanic emission fluxes for the other species were estimated by using daily species-to- SO_2 ratios and
500 either (i) interpolating the exponentially decreasing fit of SO_2 fluxes or (ii) performing a linear interpolation of



the SO₂ emission fluxes time series. The HCl, HF, CO₂ and CO volcanic emission fluxes are shown in Fig. 5 B-D, concurrently with the Time-Averaged Discharge Rate (TADR, Fig. 5E) time series of Plank et al. (2023), corrected by a factor of 2, as suggested by the authors to take the underestimation of the lava volume into account.

A significant observation is the long-term decrease in the volcanic emission fluxes of SO₂, HCl, HF, and CO, which aligns with the TADR trend throughout the eruption, in contrast to the nearly stable trend of CO₂. An excellent correlation was found (see Fig. E1) between the daily average SO₂ emission fluxes and the TADR (including 20/32 available TADR-fluxes pairs), with a slope of 14.1 ± 1.2 kg of SO₂ per thermal m³ of discharged lava (lava volumes estimated using the radiant flux) and a Pearson coefficient $R=0.94$. This relationship is mainly valid from 7 October 2021 onwards (Fig. E2). Another important observation is that the SO₂ flux peak recorded during the first week of the eruption, accounting for approximately 20% of the total SO₂ emissions, occurs during a period of low TADR and around ten days prior to the first peak with maximum values of TADR for the eruption. The relationship between the SO₂ volcanic emission fluxes and the TADR is examined in the light of the petrological data in section 5.

Furthermore, the early November peaks in the HF, HCl, and CO emission fluxes time series, which align with those observed in several ratios time series (Fig. 3), correspond to the inflection point in the overall flux decline, occurring near the end of Phase I, as defined by Milford et al. (2023). Since the CO₂ volcanic emission fluxes appear to be nearly constant throughout the entire eruptive period, we can interpret the lower HCl and HF-to-CO₂ ratios of phase II as the result of globally lower fluxes during this period, in line with the pressure decrease in the reservoir (Milford et al., 2023; Charco et al., 2024).

Table 4 presents the average volcanic emission fluxes for each species over the entire eruption distinguishing between the results from the two previously described methods. Total emissions were estimated by combining a Monte Carlo approach to account for uncertainties with trapezoidal integration to compute the area under the curve, and are also reported in Table 4. The average fluxes over the entire eruptive period and the estimated total emissions of SO₂, HCl, HF, and CO₂ (Table 4) provide insight into the scale of the emissions of this eruption with respect to other emission sources.

Table 4: Estimate of total emissions during the eruption from gas to SO₂ ratios and SO₂ emission fluxes. The emission fluxes estimates were performed using (1) exponential fit for the SO₂ emission fluxes interpolation and (2) using direct linear interpolation of SO₂ emission fluxes (results between brackets). Total emissions to the atmosphere are then derived combining the Monte Carlo and trapezoid integration methods.

Species	Average specie to SO ₂ mass ratios	Average volcanic emission fluxes (kg.s ⁻¹)	Total emissions (Mt) Estimates using exponential fit for SO ₂ volcanic emission fluxes interpolation (Estimate using direct interpolation of SO ₂ fluxes)
SO ₂	1.0	300 ± 230	1.81 ± 0.18 (1.86 ± 0.09)
CO ₂	All studies: 12 ± 10 This study: 14 ± 9	2981 ± 1105	19.4 ± 1.8 (20.5 ± 1.9)
HCl	0.03 ± 0.02	7 ± 4	0.05 ± 0.01 (0.043 ± 0.003)
HF	0.0074 ± 0.0053	1.9 ± 1.3	0.013 ± 0.002 (0.013 ± 0.002)
CO	0.09 ± 0.05	23 ± 14	0.123 ± 0.005 (0.138 ± 0.009)

The total SO₂ emissions of 1.81 ± 0.18 Mt, derived from our exponentially decreasing fit, is similar to that reported in Milford et al. (2023) using the daily SO₂ volcanic emissions derived from TROPOMI data (credit: ESA, MOUNTS). These total SO₂ emissions are comparable to the emissions of the submarine 2011 Tagoro eruption at El Hierro, that released between 1.8 and 2.9 Mt SO₂ into the ocean (estimated using the petrologic



method; see Longpré et al., 2017). The SO₂ emissions from the Tajogaite eruption are a factor of 15 higher than the total anthropogenic SO₂ emissions for Spain emitted during the year 2021 (123 kt) (MITECO, 2023) and exceed the EU anthropogenic SO₂ emissions for 2021 (1.4 Tg) (EEA, 2023). During the Tajogaite eruption, the highest SO₂ emission fluxes occurred during the first ten days of the eruption (median of 37 kt/day during this period), and then had a lower median of about 20 kt/day. These SO₂ emission rates are the same order of magnitude as the most recent basaltic eruptions such as Piton de La Fournaise in 2020 (average: 0.9 kt/day; max: 25 kt/day, Hayer et al., 2023) in La Reunion island, Bárðarbunga in 2014-2015 (average of 50 kt/day over 6 months, Pfeffer et al., 2018) in Iceland, and lower than that found at Kilauea in 2018 (average of 200 kt/day; Kern et al., 2020), but the latter two exhibiting much higher eruptive TADR. For Tajogaite, the high SO₂ fluxes result from the high sulphur content of parental magma, as reflected by the average content of 3360 ppm in our MIs (Supplementary data), similar to the value of 3500 ppm reported in Burton et al. (2023) and Dayton et al. (2024). For CO₂, we obtained a steady average emission flux of 260 ± 24 kt/day, and total emissions of 19 ± 2 Mt over the course of the eruption. This result aligns closely with the estimates of 28 ± 14 Mt reported by Burton et al. (2023). These emissions represent 15% of global subaerial volcanic and tectonic annual emissions (Fischer and Aiuppa, 2020) or the equivalent of the annual CO₂ budget of OIB volcanism, as estimated by LoForte et al. (2024). The high CO₂ emissions with respect to the low extruded magma volume during Tajogaite eruption, compared to other effusive eruptions, are explained by the extraordinarily carbon-rich magma, as it is reflected in both fluid and melt inclusions (up to 2 wt.% CO₂ in MIs; Dayton et al., 2024). This is a characteristic of Macaronesian magmas and possibly of global OIB (Burton et al., 2023; LoForte et al., 2024; Van Gerve et al., 2024). These emissions are equivalent to about 10% of the total anthropogenic CO₂ emissions for Spain in 2021 (<https://www.miteco.gob.es/es/calidad-y-evaluacion-ambiental/temas/sistema-espanol-de-inventario-sei-/informe-interactivo-inventario-nacional-emisiones-atmosfera.html>). Daily CO emissions, averaging 2 kt/day, were exceptionally high during the eruption, with a cumulative total of 0.12 ± 0.01 Mt, approximately 7% of Spain's anthropogenic CO emissions for 2021, as reported in the national inventory (1.64 Mt). Few studies in the literature have documented volcanic CO emissions, and only one (Wardell et al., 2004) has estimated CO emission fluxes during an eruption (1.74 kg/s or 0.15 kt/day at Erebus volcano) about one order of magnitude lower than what we estimated during the Tajogaite eruption. Finally, our estimated HCl and HF total emissions are about 50 ± 10 kt and 13 ± 2 kt, respectively, with an average of 604 ± 340 t/day and 173 ± 86 t/day. These emissions are in the same order of magnitude as that observed for other basaltic volcanoes, such as Etna (300-1300 t/day of HCl during the 2008-2009 eruption reported in Spina et al., 2023; 800 t/day of HCl and 200 t/day of HF in 1997 reported by Oppenheimer et al., 1998), Bárðarbunga volcano (500 t/day and 280 t/day for HCl and HF, respectively, reported in Galciczka et al., 2018). HCl and HF emissions from Tajogaite are more than an order of magnitude higher than those observed at Kilauea volcano, which reported 12-22 t/day of HCl and 6-9 t/day of HF in 2008 and 2009 (Mather et al., 2012). The Tajogaite eruption HCl total emissions are about ten times higher than the annual UK emissions since 2017 (UK National Atmospheric Inventory). They also represent approximately 20% of the total European anthropogenic emissions (Zhang et al., 2022) estimated in 2014 (220 kt) that are dominated by the energy (38% of the total emissions) and open waste burning (23% of the total emissions) sectors. This eruption total HF emissions also exceed the annual UK emissions since 2017 by a factor of 10 (UK National Atmospheric Inventory).

5. Discussion

5.1. Comparison of CO₂, CO, HCl and HF to SO₂ ratios from different measurement methods and sites

One of our key results is the remarkably strong consistency between the measured volcanic gas species-to-SO₂ ratios, whatever the measurement site, the technique and the instrument used (Fig. 3). The measurements conducted at the IZO station gave the excellent opportunity to assess the robustness of our estimated ratios, using both EM27/SUN and IFS-125HR instruments and their consistency with surface measurements. We found an excellent agreement between the HCl and HF total columns (with volcanic plume contribution) derived from the IFS-125HR and EM27/SUN products (see Appendix A for details).



We found a good comparability for the available CO_2/SO_2 and CO/SO_2 between surface and column measurements, reflecting an efficient vertical mixing. This also suggests that when the volcanic plume is detected by the surface measurements at the IZO station, the ground level concentrations are representative of the average volcanic plume composition. Since the IZO station is often located above the base height of the trade wind inversion (TWI) layer (Milford et al., 2023), volcanic plumes detected at IZO were typically transported rapidly through the low free troposphere. The progressive decrease in plume injection height throughout the eruption, combined with seasonal changes in the vertical stratification of the atmosphere (TWI height), resulted in sparse detections of the plume at the IZO station after mid-November 2021 (Milford et al., 2023). This led to a reduction of the coincident surface and total column observations.

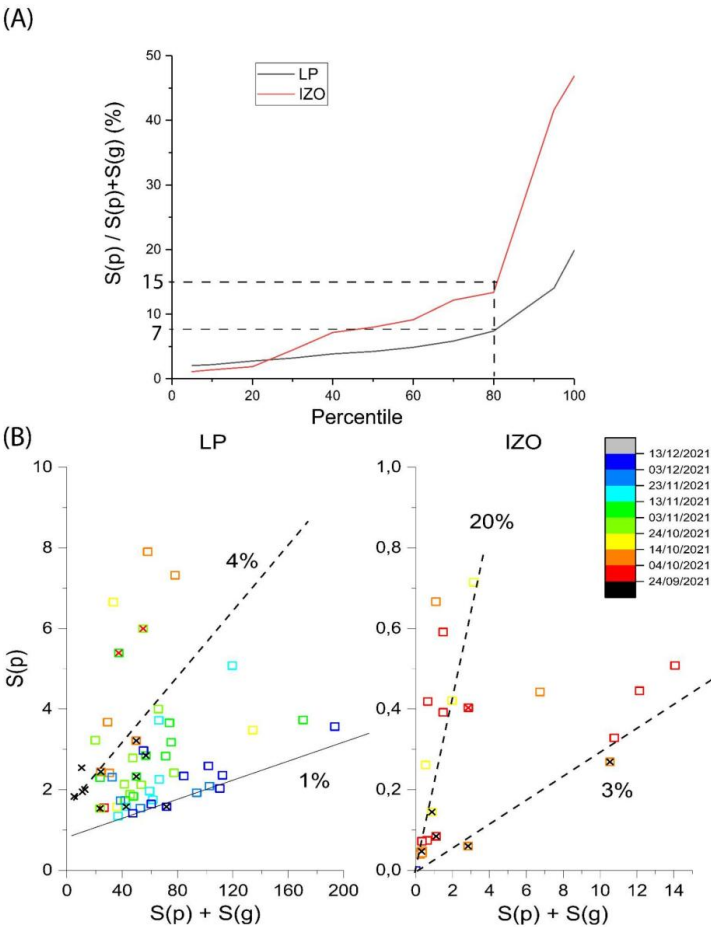
Moreover, the comparison of ratios at different distances from the eruptive vents (i) at IZO (140 km) and (ii) near the active vent measured by OP-FTIR or multiGAS (this work; Burton et al., 2023; Ericksen et al., 2024) allows qualitative assessment of the impact of in-plume reactions on our measurements. The ratios taken from Burton et al. (2023) were derived from either in situ ground-based or drone-borne multiGAS measurements within the plume close to the volcanic vents, or, after 02/10/2021, from Open-Path FTIR measurements pointing to the eruptive column and using the lava fountain as a source. Those reported by Ericksen et al. (2024) are limited to ground-based multiGAS measurements. In any case, the gas measured by these authors corresponds to the plume less than 1 km from the volcanic vents. Since CO_2 is a non-reactive species, a significant conversion of SO_2 into sulfate aerosols (H_2SO_4) during the transport between La Palma and IZO should increase the CO_2/SO_2 ratio. Hence, if significant conversion of SO_2 to sulfates occurred during the transport, the IZO ratios should be higher than those measured closer to the volcano. To examine this aspect, we estimated the plume age for each recorded event using the Hysplit transport model, in both retro-trajectories and forward simulation configuration mode. For meteorological data, we utilized 72-hour extended files containing high-resolution meteorological information derived from the WRF-ARW model as input. This model runs twice a day, using initial and boundary conditions from ECMWF's HRES-IFS data, with a resolution of $0.09^\circ \times 0.09^\circ$ (for further details, refer to Appendix C). Table 5 shows the coinciding values of the CO_2/SO_2 ratios measured at less than 1 km from the eruptive fissure (Burton et al., 2023) and at IZO (this work) and an estimate of plume age for each event. Despite the limited number of coincident events at the two distances, no clear dependence of this ratio on distance was observed for plumes with an age of 12 hours or less. Certain similarity was found, at least until the beginning of November, even in cases of relatively old plumes (~12h), suggesting a swift transport between La Palma and Tenerife islands and negligible in-plume reactions, at least indistinguishable within the uncertainties of the ratios. In the troposphere, the SO_2 to SO_4^- oxidation rates vary significantly, from a few percent per hour by in-cloud droplet processes (driven by aqueous phase oxidation e.g. H_2O_2) to a few percent per day (in dry air, driven by OH radicals) (Seinfeld and Pandis, 1998). Our results suggest that this latter (slow dry oxidation) process may be the prevailing one during the transport in the dry free-troposphere, from La Palma to IZO. This interpretation is supported by the sulphate aerosols measured in situ in La Palma (Rodríguez et al., submitted) and at IZO, when the volcanic plume reaches the station, plotted in Fig. 6. Figure 6A reports the statistical distribution of the ratio (in percent, %) of particulate sulphur (S(p), i.e. sulphate SO_4^-) over total sulphur (i.e. gas sulphur as sulphur dioxide (S(g)) plus S(p)) measured in the aerosols smaller than 10 microns (PM_{10}) at IZO and at La Palma during the eruption. Figure 6B shows the correlation plot of S(g) as a function of S(g)+S(p). We observe a higher maximum conversion rate at IZO (45%) than in La Palma (20%), as expected. However, 80% of the dataset (Fig. 6A and B) presents a conversion rate of their sulfur content to SO_4 below 15% and 7% at IZO and La Palma, respectively. Such low conversion rates would not produce resolvable differences in our gas-to- SO_2 ratios. The last two events in Table 5 present some difference between both sites. On 16 October 2021, the FTIR and surface ratios at IZO are comparable, highlighting their robustness, however, they are a factor of 2-3 lower than those reported by Burton et al. (2023). We remark that for these days, the measurement target reported by these authors mention the base of the lava fountain instead of the spattering vents or passive degassing, as for the other three dates, implying different conditions and processes.

Table 5: Comparison of the CO_2/SO_2 ratio values at two different distances from the Tajogaite eruptive centre and estimate of plume age at IZO station. FTIR ratios are given between brackets to distinguish them from surface ratios.



Date	Burton et al. (2023) Crater	IZO (140 km) Surface ratios (FTIR ratios)	Plume age at IZO (hour)
27/09/2021	6.8	7.0 ± 0.5	~8h
07/10/2021 - 08/10/2021	13	9.0 ± 0.5	~3h
13/10/2021	9;11	12.0 ± 0.3	~12h
16/10/2021 - 17/10/2021	29	10 ± 0.5 (13 ± 1)	~12h
23/11/2021 - 24/11/2021	38.3	18.3 ± 0.7	~12h

635



636

637 **Figure 6: Statistical distribution of the $S(p)$ over $S(p)+S(g)$ ratio (in percentage, p and g refers to particle and gas**
638 **respectively) measured at IZO (Tenerife) and at El Paso (La Palma) during the Tajogaite eruption. (A) shows the**
639 **statistical distribution of the conversion rate estimated from the La Palma and IZO aerosols measurements. (B)**
640 **reports $S(p)$ as a function of $S(p)+S(g)$ from the IZO and La Palma PM_{10} analysis with the time as color scale.**

641 Finally, the CO/CO_2 ratios measured at FUE station (Fig. 4) are on average higher and with higher variability
642 than those of IZO and that recently reported in Asensio-Ramos et al. (2025) from open-path measurements (Fig.



D1). This difference is likely due to the different measurements methods (solar absorption vs. open-path measurements) implying different locus of measurements and gas contribution along their respective line of sight. In particular, we note that most of the Asensio-Ramos et al. (2025) measurement sites until the beginning of November (i.e: when our highest CO/CO₂ ratios were recorded) were located at the NNW from the eruptive vent. With winds dominantly blowing towards the S and SW during this period, this configuration avoided a significant contribution of biomass and building burning plume to the measurements of these authors. It is not the case for the FUE measurements that were more likely to be affected by this contribution provoked by the advance of the lava flows. This hypothesis is also supported by the similarity of the CO/CO₂ time series at FUE with the time series of the areas covered daily by the advancing lava flows (Appendix D). The typical values reported in the literature for the wildfires (Yokelson et al., 2007; Akagi et al., 2014; Vasileva et al., 2017; Álvarez et al., 2023) are generally higher than our values, by at least a factor of 5 likely explained by the different contributors of the measured plume, i.e. a mixing of volcanic plume and vegetation/infrastructures burning in the case of the 2021 La Palma eruption. This contribution could also explain in part the difference between the FUE and IZO results, IZO only capturing the high altitude and directly transported plume, less affected by the biomass burning contribution.

5.2 New insight into the eruption dynamics

The ratios and emission flux time series as well as total emission estimates presented here provide some information about the degassing processes during the Tajogaite eruption.

Our time series of SO₂ volcanic emission fluxes confirms the preliminary decreasing trend observed from the SO₂ daily mass time series from Mounts (<http://www.mounts-project.com>, Valade et al., 2019) and reported in Milford et al. (2023). The concurrent decrease of SO₂ emissions together with that of tephra accumulation rates and plume height was suggested to reflect the decrease of the pressure in the plumbing system (Milford et al., 2023). This was confirmed by the co-eruptive deflation trend observed and inverted by Charco et al. (2024), showing the pressure drop due to drainage of the reservoir. The relatively good fit of the SO₂ fluxes data obtained using an exponential function further supports this interpretation.

The good correlation between the SO₂ volcanic emission flux time series and the TADR (slope: 14.1 ± 1.2 kg of SO₂ m⁻³ of lava and R=0.94) confirms that the emitted SO₂ mainly proceeds from the ascending magma. We observed a similar behaviour for HCl, HF and CO emission fluxes, which contrasts with the almost constant CO₂ flux throughout the 85 days of the eruption. This is in perfect agreement with the degassing model of Burton et al. (2023), depicting a decoupling between the CO₂ and SO₂ degassing processes, highlighting a significant contribution (about 80% according to Dayton et al., 2024) of a CO₂-rich volatile phase already exsolved in the upper mantle reservoir.

This duality is partially reflected in the time series of the CO₂/SO₂ ratio that steadily increases from the beginning of the eruption to the end of phase I, mimicking the trend of the VLP tremor amplitude. Such co-evolution abruptly ends at the beginning of November, from when the ratio becomes more variable. The CO₂ volcanic emission fluxes being constant within uncertainties during the whole eruption and the SO₂ volcanic emission fluxes being mainly controlled by the magma discharge rate, the steady increase of the C/S ratio during the first part of the eruption thus reflects the progressive decrease of the proportion of shallow (discharge) component relatively to the deep reservoir CO₂-rich fluids. In the frame of overall lower SO₂ fluxes due to waning activity, the variability of the ratios of the phase II reflect the control of low SO₂ contents in the plume and short-term variability of the SO₂ emissions.

The early November transition between phase I and phase II follows the apparition of new vents at the end of October (Muñoz et al., 2022), interpreted as further propagation/opening of the underlying dike intrusion. This transition shortly anticipates an abrupt and enduring drop in tremor amplitude (both VLP and LP frequency bands; Bonadonna et al., 2022), geochemical changes (Ubide et al., 2023; Dayton et al., 2024) and hydrologic and hydrochemical changes in the aquifer. The latter comprises e.g. an influx of pure (most likely endogenous) CO₂ (Jimenez et al., 2024) that drastically increased the groundwater HCO₃⁻ content at several sampling points from 27 October 2021 (Amonte et al., 2022; Garcia-Gil et al., 2023b) or the establishment of a direct relationship between the level in several groundwater wells and the tremor tremor amplitude around 7 November 2021 (Garcia-Gil et al., 2023a). VLP tremor amplitudes are especially sensitive to variations in magma ascent dynamics and conduit geometry (D'Auria et Martini, 2009; Bonadonna et al., 2022). Similar drops in VLP tremor amplitude were observed at other volcanoes, such as at Piton de la Fournaise (Duputel et



al., 2023) where it was interpreted in terms of reduction of dyke dimension, heralding the end of the eruption. All these observations suggest that these events at the beginning of November constitute a turning point in the eruption implying significant structural changes in the plumbing system.

This turning point is particularly evident with the split described in the time series in the Sr isotopic compositions of the matrix, and interpreted as the consequence of a deep-origin melt injection replenishing the feeder system (Ubide et al., 2023). This interpretation further relies on this compositional change occurring in close time relationship with an increase in the magnitude of seismicity, VLP tremor amplitude and a short-term (5 days) rebound in the time series of daily SO₂ masses. We highlight that SO₂ masses, in contrast to SO₂ emission fluxes, can be significantly affected by meteorological changes, such as ventilation decreases. Between 28 October 2021 and 2 November 2021, the ERA5 wind speed at 700 hPa was always lower than 6 m.s⁻¹ and the wind experienced a drastic change with a reversal of its direction (see e.g. Sentinel-5P TROPOMI images in Mounts time series for these days; Valade et al., 2019), which caused plume stagnation and gas accumulation. In all cases, at the depth of injection, SO₂ being mostly soluble in magma until a few hundred meters depth (Burton et al., 2023), any increase in SO₂ emissions would be due to an increase in lava discharge rate at the surface. A significant magma injection would indeed durably increase the pressure in the plumbing system, which is observed neither in the GPS baselines time series of Charco et al. (2024), nor in the TADR time series (Plank et al., 2023). This does not appear either in our CO₂ volcanic emission fluxes or composition (CO₂/SO₂) time series.

Alternatively, the observed multiparametric transition in the eruption dynamics at the beginning of November could be explained by a significant alteration of the magma pathway between the surface and the top of the magma chamber. With the waning of the eruption, the ascent rate decreased and the conduit became more unstable (Muñoz et al., 2022), with the opening of new vents from mid November (Gonzalez, 2022; Walter et al., 2023), resulting in changes in the mixing ratio and/or composition of endmembers and the return of radiogenic signatures.

5.3 Volatile mass balances and implications

Once released from the magma, volcanic gases suffer a number of processes such as oxidation, scavenging and dissolution in aqueous fluids that can alter their original composition before their detection. Integrating petrological constraints helps understanding volcanic degassing processes linking deep degassing to atmospheric observations and refining our understanding of element cycling and the environmental impact of volcanic plumes. We report here such an exercise estimating expected emissions estimated from petrological data, and compare them with our estimates derived from atmospheric measurements.

5.3.1 “Effective S degassing” and SO₂ mass balance

Combining our SO₂ volcanic emission fluxes and new petrological data, complementing literature, allow us to estimate a S degassing balance for the Tajogaite eruption. We used a similar Monte Carlo approach as proposed in Dayton et al. (2024), but refining the degassing balance as follows. We use an erupted lava volume of $(177 \pm 5.8) \times 10^6 \text{ Mm}^3$ from Civico et al. (2022), a tephra volume of $(22.8 \pm 1.8) \times 10^6 \text{ Mm}^3$ from Bonadonna et al. (2023) and a cone volume of $(36.5 \pm 0.3) \times 10^6 \text{ Mm}^3$ from Civico et al. (2022). The total erupted mass is obtained applying a similar approach to Dayton et al. (2024), using densities of $2403 \pm 170 \text{ kg.m}^{-3}$ for lava flows, based on an average percentage of vesicles for the erupted lava, 1800 kg.m^{-3} for the cone and $1200 \pm 120 \text{ kg.m}^{-3}$ for the tephra blanket (Bonadonna et al., 2022), resulting in a total erupted mass of $5.2 \times 10^8 \text{ tons}$. S degassing from the magma is usually estimated from petrological data (difference between MI and matrix glass S contents), as in the mass balance of Burton et al. (2023) and Dayton et al. (2024) for the Tajogaite eruption. The observed correlation between the TADR and our SO₂ volcanic emission fluxes allows us to directly relate the degassed volume and the emitted S mass, with $14.1 \pm 1.2 \text{ kg SO}_2$ emitted per “thermal” cubic meter of lava (lava volumes estimated using the radiant flux). We corrected this thermal volume for the tephra volume (blanket and cone) representing ~33% of the total emitted volume, because this does not participate significantly in the radiant flux. This resulted in $9.4 \pm 0.8 \text{ kg degassed SO}_2$ per cubic meter of emitted lava, which converts into $2611 \pm 285 \text{ ppm}$ effective S degassing, considering above density and a correction of the crystal mass fraction (25% following Dayton et al., 2024). This value is very similar to that obtained by Dayton et al. (2024) using the difference between the S content of inclusions ($3062 \pm 500 \text{ ppm}$) and matrix glasses ($345 \pm 53 \text{ ppm}$). Note that the average matrix S contents we present (534 ppm ; $N=52$; $\sigma=130 \text{ ppm}$; Supplementary



Table S1) and those previously published for the eruption (403 ppm; $N=438$; $\sigma=10$ ppm; Burton et al., 2023; Longpré et al., 2025) are substantially higher than the average reported by Dayton et al. (2024). Using these values in the MonteCarlo degassing simulation of Dayton et al. (2024), the full degassing of 0.25 km^3 of magma would produce emissions of 1.93 ± 0.21 Mt SO_2 . This is still slightly higher than the TROPOMI-derived total SO_2 emissions (1.81 ± 0.18 Mt).

A possibly unaccounted repository for initial S in the degassing balance could be sulfide droplets, previously described in González-García et al. (2023), exsolved from the melt during pre-eruptive crystallization and also absent from the matrix. Sulfide content has been estimated to be 0.03 vol.% (Pankhurst et al., 2022). Assuming their density is 4500 kg.m^{-3} (Saumur et al., 2015), and considering the average S content of ~35% in the analyzed sulfides (Figure S3), the potential sulfide cargo in eruptive products from the early stage of the eruption could represent ~30 kt of non-degassed S (equivalent to ~60 kt of SO_2). This would further improve the agreement between the petrologic budget (1.87 Mt of SO_2) and satellite measurements (1.81 ± 0.18 Mt of SO_2).

Surprisingly, applying the same approach for the first week of the eruption (LU1 in Bonadonna et al., 2023) encompassing the TROPOMI-derived SO_2 emission peak, we observe a mismatch of a factor of 3 between the expected SO_2 degassing and that measured by TROPOMI. This arises from the very low thermal lava volume (4.3 Mm^3 , corrected with the factor of 2 recommended by Plank et al., 2023), which can be due to the transient time required for the surface thermal structure to become steady (Coppola et al., 2016). Using alternatively the cumulative volume of $43.0 \pm 6.1\text{ Mm}^3$ on the 26-09-2021 reported by Belard and Pinel (2022) and derived from multiple Pléiades stereoscopic surveys during the first period of the eruption), and assuming a volume of the edifice of and volume of edifice of 15 ± 0.12 (Romero et al., 2022). We found cumulated SO_2 emissions of about 580 ± 66 kt, which is closer to the TROPOMI-derived estimates for this period (about 560 kt).

5.3.2 CO_2 mass balance and reservoir melt fraction

Applying the same MonteCarlo approach for CO_2 and assuming full degassing, about 4.4 ± 0.8 Mt of CO_2 would have been degassed from the erupted material alone, which is similar to Dayton et al. (2024) estimate of 5.4 ± 1.0 Mt. The significantly higher (19.4 ± 1.8 Mt) CO_2 emissions measured at the surface and the almost constant fluxes during the entire eruption strongly support the existence of a CO_2 -saturated melt in the reservoir coexisting with a CO_2 -rich fluid phase (Burton et al., 2023), that would produce emissions of the order of magnitude of 15 Mt. We used the lowest FI densities ($\sim 750\text{ kg.m}^{-3}$, corresponding to depths of ~15km) measured by Dayton et al. (2023) to calculate the volume of this fluid phase accumulated on top of the reservoir, such as defined by the shallow seismic cluster (D'Auria et al. 2022; Del Fresno et al. 2023) and the deflation source of Charco et al. (2024). At such conditions, 19.4 Mt of CO_2 would correspond to a total volume of about 26 Mm^3 . The volume extracted from the reservoir can be calculated as follows 1) correcting the eruptive products volume for its vesicularity (Dense Rock Equivalent or DRE volume, taking as a reference a melt density of $\sim 2700\text{ kg.m}^{-3}$; see Dayton et al., 2024), 2) adding the volume of the magma-filled dykes and sill network (as described by De Luca et al., 2022) and 3) finally, correcting for the effect of magma compressibility. According to Rivalta and Segall (2008), the volume ratios (intrusion/associated reservoir deflation) necessary to estimate magma compressibility range between 1.2 and 7.7. For the Tajogaite eruption, the most likely value is ~5 (reservoir 10-15 km deep, saturation depth >25 km; see their Figure 3). Using such values allows estimating a total volume extracted from the reservoir of $\sim 50\text{ Mm}^3$ (30-210 Mm^3 for the full range of volume ratios). Charco et al. (2024) show that the pressure decrease in the reservoir at the end of the eruption is of about 1% with respect to pressure at eruption onset. Assuming that this 1% pressure loss corresponds to the volume change due to the extraction of this melt volume from the mantle reservoir, we roughly estimate the volume of “volatiles+melt” in the reservoir to equate, at least to 5 km^3 (3-21 km^3 range). This volume would represent a melt fraction of ~1.5% for the “magma-filled rock volume” with the geometry extending between 7 and 25 km b.s.l. as described by D'Auria et al. (2022), and corresponding to a volume with lower seismic velocities ($V_p/V_s > 1.98$).

5.3.3 Halogens mass balance

Fluorine and chlorine did not degas significantly from the melt, because the difference between the MI and matrix glass Cl content is hardly resolvable from analytical uncertainty (Dayton et al., 2024). We thus



assessed the consistency of our fluxes using another approach, estimating the expected Cl and F degassed amount from the total observed emissions.

The adsorption of halogen-derived salts onto ash surfaces is likely to be a non-negligible sink for hydrogen halides of the volcanic plume (Bagnato et al., 2013) and should be considered in our balance. We thus propose a rough estimate of the scavenged halogen mass using the median (and standard error) content of Cl (335 ± 34 ppm) and F (422 ± 49 ppm) from a compilation ($N=57$) of published lixiviation experiments (Ruggieri et al. 2023; Sanchez-España et al., 2023; Rodriguez et al., 2025, submitted) and the mass of tephra emitted throughout the eruption (Bonadonna et al., 2022), including the cone (Civico et al., 2022). We obtain estimates of 31 ± 8 kt HCl and 39 ± 11 kt HF possibly scavenged from the plume, that we need to sum to our measured HCl and HF budgets (49 ± 12 kt and 13 ± 2 kt of HCl and HF, respectively), giving surface emissions of 80 ± 15 and 52 ± 11 kt for HCl and HF, respectively.

Using the average Cl and F contents in MIs of Dayton et al. (2024), these emissions can be explained with Cl and F losses of ~ 195 and 130 ppm from the melt, respectively. This is 35% and 9% of the initial melt content in Cl and F, respectively. This Cl difference should be resolvable analytically, but the F difference is indeed within the analytical uncertainty of electron microprobe for volcanic glasses (Rose-Koga et al., 2021) and at the limit of that for the Secondary Ion Mass Spectrometry analyses of Dayton et al. (2024). We propose a complementary estimation of the Cl loss from the melt using petrological data of the MI and matrix glasses of the eruption (Burton et al., 2023; Dayton et al., 2024; Longpré et al., 2025). The determination of the amount of Cl degassing from the melt is indeed obscured by the magma evolution in the plumbing system, as shown by the bivariate diagram between K_2O and the Cl contents (Fig. B2A), where the matrix glass Cl contents are consistently higher than that of MI, impeding simple quantifications by difference as for S balance. In this diagram, MIs define a trend (Pearson's $R=0.943$) that can be used to estimate the average Cl amount degassed from magma. We find an error-weighted mean Cl content difference between the simulated undegassed magma compositions and the matrix glasses of 189 ± 10 ppm (95%; $N=633$; $\sigma=135$), within uncertainties of our degassing balance approach. The total HCl emissions that would arise from such degassing from the volume of eruptive products is 77 ± 7 kt, indistinguishable from our HCl balance of 80 ± 15 kt within uncertainties. This approach is not possible for F due to significant variability in MI F content.

6. Summary and Conclusion

In this study, we explored the variability of the chemical composition of the Tajogaite volcanic gas plume by combining ground-based FTIR and UV direct-sun measurements with surface gas observations at two sites: Fuencaliente, on La Palma, and the Izaña high-altitude Atmospheric Observatory, a reference station for atmospheric studies located in Tenerife. New retrieval methods are presented to derive the HF and HCl volcanic contribution in the total columns obtained from the solar FTIR spectra for both low (EM27/SUN) and high (IFS-125HR) spectral resolution measurements performed up to 140 km from the eruptive fissure. The good agreement between the different products (total columns and ratios) obtained from the different instruments (FTIR, DOAS and surface measurements) demonstrates the robustness of our results, even at such distant and low-concentration locations as the 140 km-far IZO Observatory. Our compositional ratios measured during the eruption are also consistent with the limited data reported in the literature (Asensio-Ramos et al., 2025; Ericksen et al., 2024; Burton et al., 2023), including for previous basaltic eruptions in the world (e.g. Aiuppa et al., 2009). We derived SO_2 volcanic emission fluxes from the TROPOMI data and assessed the long-term variability of the emission fluxes of the other volcanic species, based on our compositional data. We found total emissions of SO_2 , CO_2 , HCl, HF and CO of 1.8 ± 0.2 , 19.4 ± 1.8 , 0.05 ± 0.01 , 0.013 ± 0.002 and 0.123 ± 0.005 Mt, respectively. These emissions were found to be non-negligible in the annual Spanish national and European inventory balance compared to anthropogenic emissions. Furthermore, while the SO_2 and halogen halides volcanic emission fluxes decreased along with the eruption, the CO_2 volcanic emission fluxes were found to be almost constant, confirming the dual behaviour of the degassing source, as previously observed by Burton et al. (2023). As our SO_2 volcanic emission fluxes present a good correlation with the lava emission fluxes, CO_2 emissions are decoupled from the volcanic emissions and arise from the deep reservoir. Finally, global degassing balances were performed for C, S, Cl and F, showing a good consistency between the plume measurements and the petrological data. This study highlights the potential of employing existing global atmospheric FTIR, DOAS and surface measurement networks to explore remotely (>100 km) the variability of volcanic plumes chemical



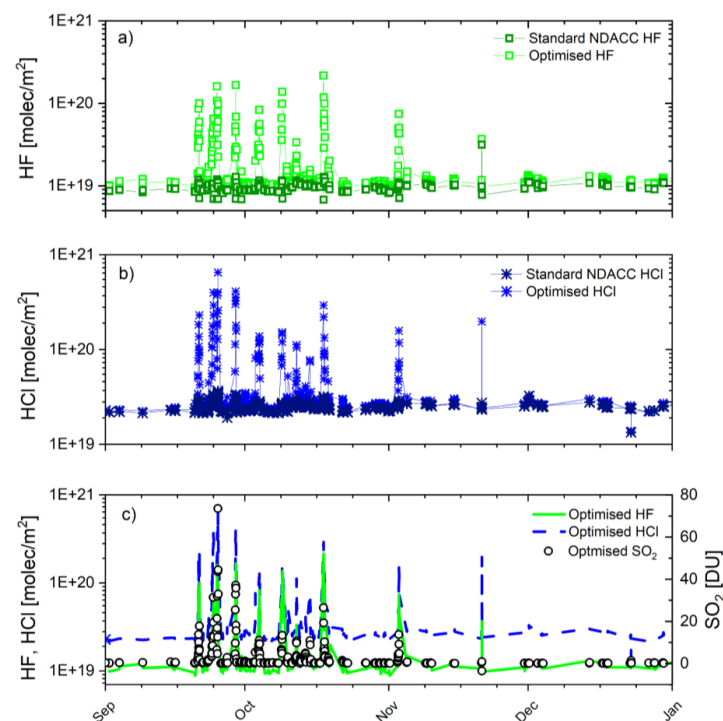
composition and its implications at different timescales. By demonstrating their effectiveness in tracking volcanic emissions in real time, our findings underscore the value of these networks for both operational volcano monitoring and scientific investigations during eruptive crises. Such measurements are crucial for assessing the role of volcanic emissions as natural sources in the global cycling of carbon, sulfur, and halogens. This study emphasises the value of solar absorption measurements for volcanology, atmospheric research, and air-quality monitoring during eruptions, and suggests their potential application during major eruptions even when access is more restricted.

7. Appendices

Appendix A

Comparison between the new HF and HCl products derived from the IFS-125HR and EM27/SUN measurements

The appendix A provides a summary of the comparison between the standard NDACC FTIR HCl and HF products and those developed in this study, the new IFS-125HR SO₂ retrievals (Fig. A1), as well as the comparison between all the IFS-125HR and EM27/SUN products (Fig. A2). As illustrated by the comparison (Table A1), the standard and optimised approaches show an excellent agreement under background conditions with a mean bias of approximately 3% and 15% for HCl and HF, respectively, while the scatter is limited to 4% for both trace gases. These values fall within the expected uncertainty estimations of the IFS-125HR products (García et al., 2021). However, for volcanic emissions, the NDACC approaches, in contrast to our optimized approach, are not able to capture the volcanic HCl and HF contributions in the lower/middle troposphere, resulting in a mean difference of 88% and 100% for HCl and HF, respectively. Column enhancements as large as 6.00×10^{20} and 2.05×10^{20} molec/m² for HCl and HF, respectively, were reported during the volcanic process, which accounts for the high variability observed between mean, median and scatter values under volcanic emissions.





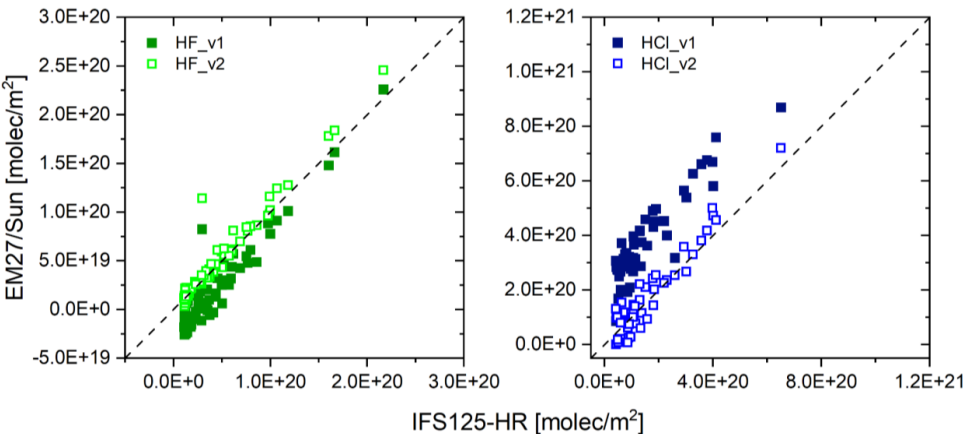
871 **Figure A1: Time series of the standard NDACC and optimised HF (a) and HCl (b) total column amounts measured at**
872 **IZO from the IFS-125HR instrument between 1 September and 31 December 2021. (c) Time series of the optimised**
873 **HF, HCl and SO₂ IFS-125HR products at IZO for the same period.**

874 Figure A1 also presents the SO₂ total column amounts retrieved from the IFS-125HR measurements at IZO. The
875 excellent agreement found between the SO₂, HCl and HF retrievals consistently capturing volcanic plumes
876 probes the reliability and quality of the optimised IFS-125HR products, which has been also documented by
877 side-by-side Pandora and FTIR SO₂ observations (Taquet et al. 2023). As found for the NDACC FTIR sites of
878 IZO and Altimoni (García et al., 2022), the Pandora and FTIR comparison shows an excellent correlation for
879 the whole SO₂ range observed (Pearson correlation coefficients larger than 0.99) and the scatter between
880 techniques is comparable to background signal (less than 0.7 and 2.0 DU for IZO and Altimoni, respectively).
881 For further details about SO₂ IFS-125HR retrieval refer to García et al., (2022, in prep).

882 **Table A1: Summary of the comparison between the standard NDACC and optimised HF and HCl total column**
883 **amounts measured at IZO from the IFS-125HR instrument for the period (1) 1-15 September and 1-31 December**
884 **2021 under background conditions; and (2) between 19 September and 31 November affected by volcanic emissions.**
885 **N stands for the number of measurements and STD corresponds to the standard deviation of the data distribution.**

	Background conditions (1-15 September & 1-31 December, N=68 for HCl and N=67 for HF)			Volcanic emissions (19 September - 31 November, N=414 for HCl and N=405 for HF)		
IFS-125HR Products	Mean	Median	STD	Mean	Median	STD
NDACC HCl [molec.m ⁻²]	2.47E19	2.50E19	1.46E18	2.47E19	2.40E19	2.69E18
Optimised HCl [molec.m ⁻²]	2.55E19	2.57E19	2.02E18	5.07E19	2.7E19	6.86E19
NDACC - Optimised HCl [molec.m ⁻²]	8.11E17	7.49E17	9.79E17	2.60E19	2.88E18	6.66E19
NDACC - Optimised HCl [%]	3.2	3.0	3.9	88	12	204
NDACC HF [molec.m ⁻²]	9.92E18	9.77E18	6.85E17	9.51E18	9.19E18	1.46E18
Optimised HF [molec.m ⁻²]	1.14E19	1.14E19	6.95E17	1.95E19	1.12E19	2.34E19
NDACC - Optimised HF [molec.m ⁻²]	1.50E18	1.45E18	3.64E17	1.00E19	1.68E18	2.32E19
NDACC - Optimised HF [%]	15.2	14.9	4.1	100	18	288

886 Figure A2 shows the comparison between the new HCl and HF products (HCl_v2 and HF_v2) derived from the
887 EM27/SUN measurements, as well as those (HCl_v1 and HF_v1) estimated using the same retrieval as Butz et
888 al. (2017) and the new products derived from the IFS-125HR measurements at IZO. Fit parameters are
889 presented in Table A2. An excellent correlation was found for the newly developed EM27/SUN products
890 (HCl_v2 and HF_v2), highlighting the improvements of the retrieval methods especially in case of far
891 measurement sites.



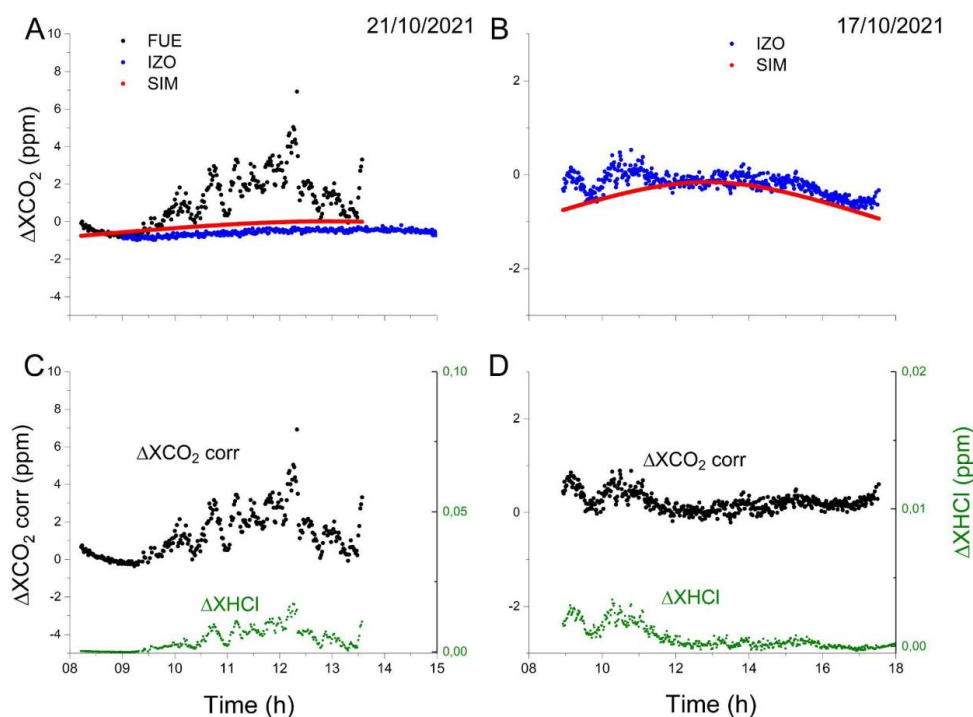
892
893 **Figure A2: Intercomparison between the IFS-125HR and EM27/SUN HF and HCl total columns obtained from side-**
894 **by-side measurements during the Tajogaite eruption. The diagonal ($y=x$) is plotted as a dashed line. The fit**
895 **parameters from linear regression are given in Table A2.**

896 **Table A2: Fit parameters obtained from the linear regression between the EM27/SUN HF and HCl products and**
897 **those from the IFS-125HR.**

EM27/Sun (10 min average centered in the IFS125-HR measurements) vs. IFS-125HR	Linear regression using least squares fitting method
HF_v1	Slope= 1.11 ± 0.03 Offset= $(-2.7 \pm 0.2) \times 10^{19}$ molec/m ² R=0.91
HF_v2	Slope= 1.11 ± 0.025 Offset= $(-2.0 \pm 11.8) \times 10^{17}$ molec/m ² R=0.98
HCl_v1	Slope= 1.14 ± 0.07 Offset= $(20.4 \pm 1.5) \times 10^{19}$ molec/m ² R=0.92
HCl_v2	Slope= 1.11 ± 0.05 Offset= $(-0.43 \pm 1.07) \times 10^{19}$ molec/m ² R=0.95

898
899 **Procedure for removing CO and CO₂ background to the total column estimates and extracting volcanic**
900 **contribution**

901 CO and CO₂ analysis from the total column measurements require the simulation and removal of the
902 background concentration. Figure A3 shows the procedure we employed for this study, through two examples
903 from the FUE and IZO dataset. The time series is first detrended from the annual cycle, using IZO long-term
904 time series and a third degree polynomial. The intraday variability of CO₂ background is then simulated using
905 the average of the XCO₂ intraday time series from spectra without volcanic plume contribution. The background
906 contribution is simulated for each day, fitting an offset. An example of the total procedure is illustrated in Fig.
907 A3. The simulated background at FUE (in red, A) was compared with IZO measurements (in blue, A) when it
908 was not affected by the volcanic plume. The resulting intraday time series of ΔXCO_2 (Fig A3C and A3D) in
909 presence of volcanic plume is well correlated with the ΔHCl , which can be considered as a tracer of the volcanic
910 plume.

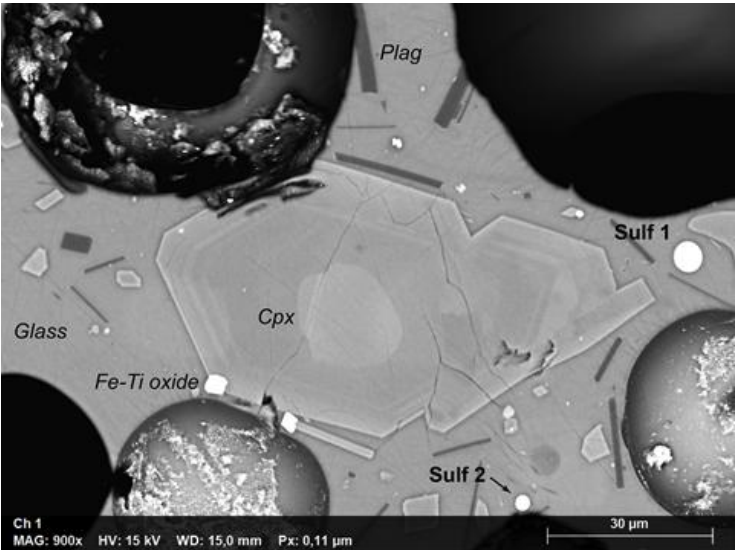


911
912 **Figure A3:** Procedure for removing the atmospheric background contribution to estimate the CO_2 and CO
913 abundance in the volcanic plume. A and B show a typical example of uncorrected ΔXCO_2 at FUE (in black) and IZO
914 (in blue) and the corresponding simulated background (red). The background simulations (in red) obtained using the
915 average diurnal pattern without presence of volcanic plume and adjusting offset is compared with the measurements
916 taken at the IZO station (blue) on the same day. The corrected ΔXCO_2 is presented in black in (C) and (D)
917 concurrently with the $\Delta XHCl$, which can be considered as a tracer of the volcanic plume.



918 **Appendix B**

919 Appendix B presents the tephra compositions acquired with Scanning Electron Microscope and Electron Micro-
920 Probe and used in the petrologic approach of the estimation of the volatile emissions.



	S	Fe	Ni	Cu
Sulf1	35.7	54.2	2.9	7.3
Sulf2	34.6	53	2.8	9.7

921

922 **Figure B1:** Scanning electron microscope image of a section of LM-2309 tephra sample (Gonzalez-Garcia et al., 2023)
923 displaying two sulfide droplets. The BSE images were acquired using a JEOL JSM-7610F gun emission scanning
924 electron microscope. The table below shows their compositions (in wt%), determined by energy dispersive
925 spectroscopy with a Cameca SX-100 electron microprobe.

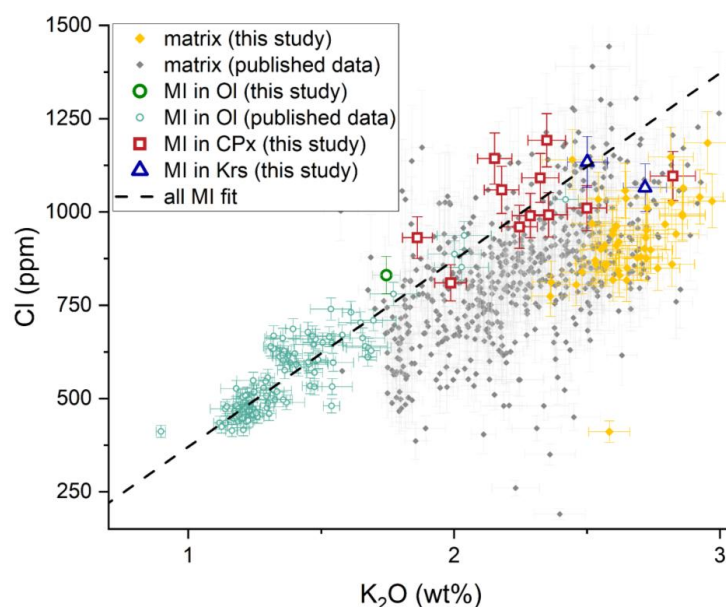


Figure B2: New and previously published Cl content in MIs (green hollow circles) and matrix glass (orange diamonds) with melt evolution, represented by the incompatible K_2O . MI compositions are from this study, Burton et al. (2023) and Dayton et al. (2024). OI stands for olivine, CPx, for clinopyroxene and Krs for Kaersutite. Matrix glasses are from this study, Burton et al. (2023), Ubide et al., 2023, Dayton et al. (2024), Longpré et al. (2025). The dashed line is the linear regression through the MIs dataset and represents the increase in melt Cl content during crystal fractionation. We calculated the degassed Cl amount as the error-weighted mean difference between each matrix Cl content and the regression line.

Appendix C

Appendix C details the procedure that we employed to estimate the plume age for the dates reported in Table 5, using the Hysplit forward simulations.

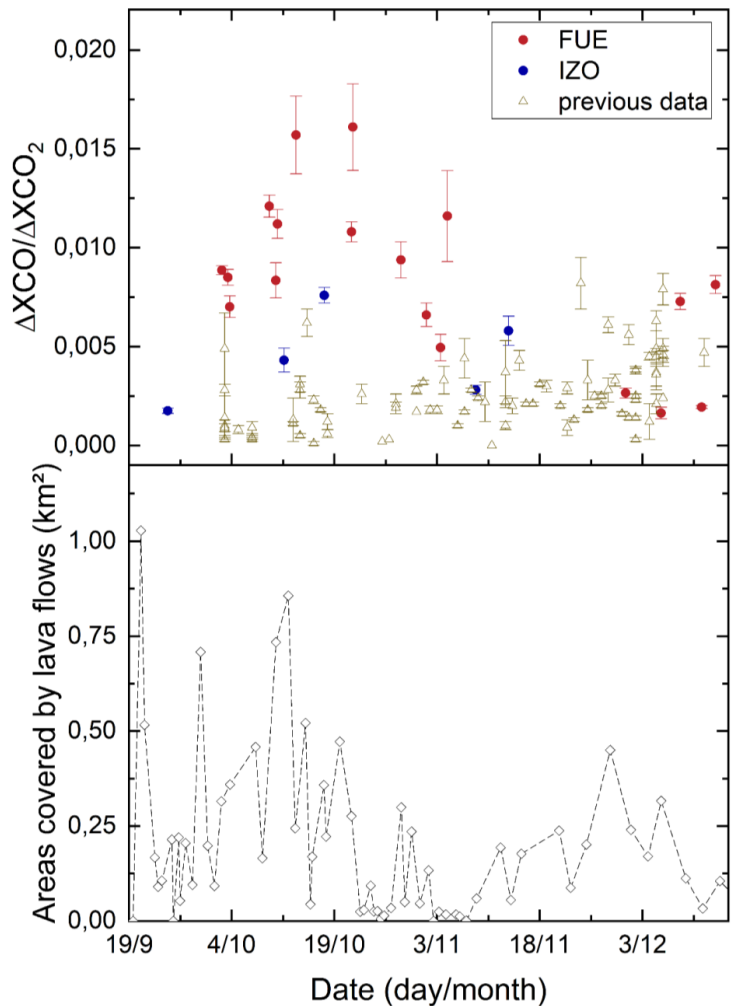
We used high resolution meteorological data derived from the WRF-AWR (Advanced Research Weather Research and Forecasting) model (Powers et al., 2017; Skamarock et al., 2019). The WRF-ARW model is run operationally twice daily, utilizing initial and boundary conditions from HRES-IFS (High Resolution Integrated Forecast System) data provided by ECMWF (European Centre for Medium-Range Weather Forecasts) at a resolution of $0.09^\circ \times 0.09^\circ$. The model configuration includes three nested domains with horizontal resolutions of 6 km, 2 km, and 1 km, respectively, and 31 vertical levels, operating in non-hydrostatic mode. Each simulation produces forecasts extending up to 72 hours. The outputs of the WRF-ARW model are converted into the required format for the HYSPLIT model (Hybrid Single-Particle Lagrangian Integrated Trajectory) using the ARW2ARL program. This process produces meteorological data formatted for use in trajectory and dispersion simulations. To prepare the data for HYSPLIT, the WRF-ARW outputs are processed to generate ARL files with a 12-hour temporal span. These files are designed to overlap every 12 hours, ensuring continuous hourly meteorological data coverage. This approach provides a seamless dataset necessary for accurate and uninterrupted backward trajectory and forward simulation calculations. Forward simulations were performed using Hysplit with a standard configuration over a minimum total calculation time of 48h and an hourly time resolution. The plume altitude was taken from the IGN/AEMET data and Milford et al. (2023) for each studied date.

Appendix D

Appendix D presents the comparison between the $\Delta XCO/\Delta XCO_2$ measured at FUE and IZO using the direct-sun FTIR measurements and the area covered daily by the lava flows, derived from the daily Copernicus



956 EMSR546 mapping. A good agreement is found between the two dataset, indicating a possible contribution of
957 the burning infrastructure and vegetation in our FUE FTIR measurements. It contrasted with the ratios reported
958 by Asensio-Ramos et al. (2025) derived from open-path measurements performed at the N-NW from the
959 eruptive fissure, less affected by this contribution.



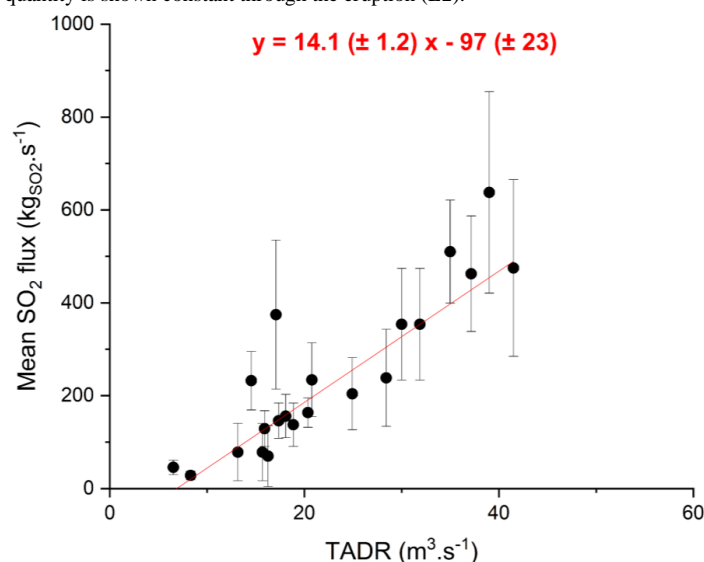
960

961 Figure D1: Comparison between the time series of $\Delta XCO/\Delta XCO_2$ ratios obtained over the whole eruptive period and
962 the daily covered area by the lava flows derived from the daily Copernicus EMSR546 mapping ([COPERNICUS](#)
963 [EMERGENCY MANAGEMENT SERVICE | Copernicus EMS - Mapping](#)). In the upper subset, the ratio calculated
964 from the IZO and FUE FTIR measurements are presented by blue and red circles, while the ratios reported in
965 Asensio-Ramos et al. (2025) are presented by hollow triangles.

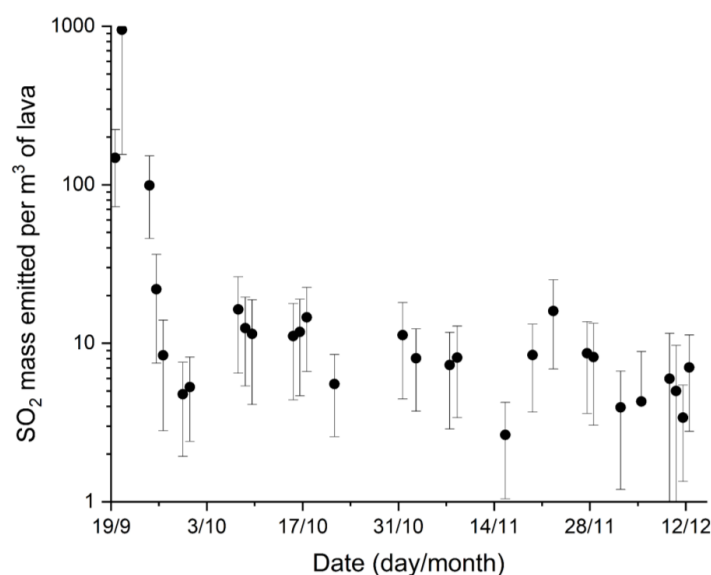


966 Appendix E

967 Appendix E describes the relationship observed between the retrieved daily SO₂ emission fluxes and the lava
 968 Time Averaged Discharge Rate (TADR). The TADR estimates the lava volume responsible for the radiant flux
 969 measured by satellite (Coppola et al., 2016). We exploit the fact that this volume is also the source of SO₂
 970 emissions (Fig. E1), providing a direct quantification of the amount of S actually degassing (“effective S
 971 degassing”), which is usually indirectly derived a posteriori, by the difference between the S content of the
 972 primitive magma (melt inclusions) and that remaining in the matrix of the (degassed) eruptive products. This
 973 quantity is shown constant through the eruption (E2).



974
 975 Figure E1: Correlation between the TADR and SO₂ volcanic emission fluxes illustrating an average “effective S
 976 degassing” of 14.1 ± 1.2 kgSO₂ per (thermal) cubic meter of lava discharged to the surface.



977
 978 Figure E2: Time series of “effective S degassing”.



979 **8. Data availability**

980 FTIR data used in this study are available upon request. In situ surface data at Izaña
981 Atmospheric Observatory contribute to the WMO-GAW Programme and are available at the World
982 Data Centre for Greenhouse Gases (WDCGG, <https://gaw.kishou.go.jp/>). TROPOMI data
983 (Copernicus Sentinel-5P) are publicly available from Sentinel-5P data hub at
984 https://sentinels.copernicus.eu/web/sentinel/data-products/-/asset_publisher/fp37fc19FN8F/.
985 Petrological dataset is available as Supplementary Material.

986 **9. Authors contribution**

987 All of the co-authors contributed to the preparation and writing of the manuscript. OG, TB,
988 NT conceptualised the study. OG led the development of the FTIR program at the Izaña Atmospheric
989 Observatory and its long-term operation. OG, RR, AA, VC were in charge of the implementation and
990 operation of the Fuencaliente (La Palma) station during the eruption. They also assured the operation
991 and maintenance of measurements at IZO. OG, NT, WS, ES, SL contributed to the FTIR and DOAS
992 and data analysis. SL and PRS are responsible for the GAW surface measurements at IZO and their
993 processing. NT, TB, RC, WS, OG contributed to the implementation and operation of the combined
994 DOAS-EM27/SUN measurements at Fuencaliente. NT, TB, RC performed the multiGAS
995 measurements and ash sampling. RC processed the multiGAS data. DGG, AK performed the SEM
996 and EPMA analyses and helped for the interpretation and discussion of results. CA, MIG contribute to
997 realisation of the Hysplit modelling of the volcanic plume dispersion to estimate the plume age. SR,
998 JLD performed the chemical analysis of the PM₁₀ and contributed to their interpretation. MIG, SR,
999 PGS, TB, NT contribute to the discussion about the PM₁₀ measurements. FH helped with the FTIR
1000 operating maintenance and data processing. He developed the PROFFAST and PROFFIT retrieval
1001 codes and provides continuous support to the group with respect to its use and spectrometer operation.
1002 FH and OG led the German–Spanish collaboration and provided precious help with respect to the
1003 EM27/SUN measurements within the framework of the COCCON network.

1004 **10. Acknowledgments**

1005 The AEMET team and TB acknowledge the San Antonio volcano visitor's center in
1006 Fuencaliente and its personnel for authorizing and facilitating the instrumentation deployment there.
1007 The AEMET team also would like to thank all the researchers and technical personnel for the
1008 maintenance and operation of the instrumentation at the Izaña Atmospheric Observatory. The CSIC
1009 team and RC acknowledge the administration of the IPNA-CSIC and the CSIC deployment plan
1010 during the eruption and its coordination by Manuel Nogales. NT is grateful to the IPNA-CSIC and its
1011 director, Juan Ignacio Padron Peña, for allowing her temporary research internship during the
1012 eruption. TB, NT, RC, DGG and AK are grateful to PEVOLCA for granting permission for access to
1013 the exclusion zone during sampling and to F.M. Medina from the Cabildo Insular de La Palma for the
1014 sampling authorizations and for facilitating the fieldwork campaigns. TB and NT acknowledge Pablo
1015 González (Group of Volcanology of IPNA-CSIC) and A. Barreto (Aerosols group from the CIAI-
1016 AEMET) for the fruitful discussions and M. Charco (IGEO-CSIC, Madrid) for providing the
1017 corrected lava emission volumes data. Authors are grateful to S. Valade for the SO₂ masses from
1018 Mounts Project. NT, RC, and TB acknowledge C. Fayt, M. Van Roozendaal, and A. Merlaud from the
1019 BIRA-IASB institute for providing and helping with the use of QDOAS software. The CSIC team and
1020 R.C. acknowledge the Cabildo Insular de La Palma and its personnel for their assistance in the field.



1021 They also warmly thank J.G. Barreto from Spar La Palma and TICOM solutions and his personnel for
1022 their logistic support and assistance in the field.

1023 **11. Financial Support**

1024 This study was partially funded by the European Union – NextGenerationEU within the
1025 actions P02.C05.I03.P51.S000.42 and P02.C05.I03.P51.S000.43. This study is part of the projects
1026 AERO-EXTREME (PID2021-125669NB-I00), funded by the Spanish National Research Agency
1027 (Agencia Estatal de Investigación) and the European Regional Development Funds. This study has
1028 received funding from the European Union’s Horizon Europe Research and Innovation programme
1029 under Grant Agreement 101189654. DGG acknowledges financial support from the Alexander von
1030 Humboldt Foundation through a Humboldt Fellowship for Postdoctoral Researchers. This work
1031 benefited from funding from CSIC and the Ministry of Science and Innovation through the CSIC-PIE
1032 project PIE20223PAL009. The aerosol sampling in La Palma during the eruption and part of the
1033 chemical analysis were performed within the framework of the project CSIC-LAPALMA-06, funded
1034 by CSIC and the Ministry of Science and Innovation.

1035 **12. References**

- 1036 ACTRIS, ACTRIS-Spain coordinating unprecedented actions for the Cumbre Vieja volcanic emergency,
1037 November 2021. Available at: [https://www.actris.eu/news-events/news/actrispain-coordinating-unprecedented-](https://www.actris.eu/news-events/news/actrispain-coordinating-unprecedented-actions-cumbre-viejavolcanic-emergency)
1038 [actions-cumbre-viejavolcanic-emergency](https://www.actris.eu/news-events/news/actrispain-coordinating-unprecedented-actions-cumbre-viejavolcanic-emergency)
1039
- 1040 Akagi, S. K., Burling, I. R., Mendoza, A., Johnson, T. J., Cameron, M., Griffith, D. W. T., Paton-Walsh, C.,
1041 Weise, D. R., Reardon, J., and Yokelson, R. J.: Field measurements of trace gases emitted by prescribed fires in
1042 southeastern US pine forests using an open-path FTIR system, *Atmos. Chem. Phys.*, 14, 199–215,
1043 <https://doi.org/10.5194/acp-14-199-2014>, 2014.
- 1044 Alberti, C., Hase, F., Frey, M., Dubravica, D., Blumenstock, T., Dehn, A., Castracane, P., Surawicz, G., Harig,
1045 R., Baier, B. C., Bès, C., Bi, J., Boesch, H., Butz, A., Cai, Z., Chen, J., Crowell, S. M., Deutscher, N. M., Ene,
1046 D., Franklin, J. E., García, O., Griffith, D., Grouiez, B., Grutter, M., Hamdouni, A., Houweling, S., Humpage,
1047 N., Jacobs, N., Jeong, S., Joly, L., Jones, N. B., Jouglet, D., Kivi, R., Kleinschek, R., Lopez, M., Medeiros, D. J.,
1048 Morino, I., Mostafavipak, N., Müller, A., Ohyama, H., Palmer, P. I., Pathakoti, M., Pollard, D. F., Raffalski, U.,
1049 Ramonet, M., Ramsay, R., Sha, M. K., Shiomi, K., Simpson, W., Stremme, W., Sun, Y., Tanimoto, H., Té, Y.,
1050 Tsidu, G. M., Velasco, V. A., Vogel, F., Watanabe, M., Wei, C., Wunch, D., Yamasoe, M., Zhang, L., and
1051 Orphal, J.: Improved calibration procedures for the EM27/SUN spectrometers of the COllaborative Carbon
1052 Column Observing Network (COCCON), *Atmospheric Measurement Techniques*, 15, 2433–2463,
1053 <https://doi.org/10.5194/amt-15-2433-2022>, 2022.
- 1054 Álvarez, Ó., Barreto, Á., García, O. E., Hase, F., García, R. D., Gröbner, J., León-Luis, S. F., Sepúlveda, E.,
1055 Carreño, V., Alcántara, A., Ramos, R., Almansa, A. F., Kazadzis, S., Taquet, N., Toledano, C., and Cuevas, E.:
1056 Aerosol properties derived from COCCON ground-based Fourier Transform spectra,
1057 <https://doi.org/10.5194/amt-2023-106>, 30 June 2023.
- 1058 Amonte, C., Melián, G. V., Asensio-Ramos, M., Pérez, N. M., Padrón, E., Hernández, P. A., and D’Auria, L.:
1059 Hydrogeochemical temporal variations related to the recent volcanic eruption at the Cumbre Vieja Volcano, La
1060 Palma, Canary Islands, *Front. Earth Sci.*, 10, 1003890, <https://doi.org/10.3389/feart.2022.1003890>, 2022.
- 1061 Asensio-Ramos, M., Cofrades, A. P., Burton, M., La Spina, A., Allard, P., Barrancos, J., Hayer, C., Esse, B.,
1062 D’Auria, L., Hernández, P. A., Padrón, E., Melián, G. V., and Pérez, N. M.: Insights into magma dynamics from
1063 daily OP-FTIR gas compositions throughout the 2021 Tajogaite eruption, La Palma, Canary Islands, *Chemical*
1064 *Geology*, 676, 122605, <https://doi.org/10.1016/j.chemgeo.2024.122605>, 2025.



- 1065 Bagnato, E., Aiuppa, A., Bertagnini, A., Bonadonna, C., Cioni, R., Pistolesi, M., Pedone, M., and Hoskuldsson,
1066 A.: Scavenging of sulphur, halogens and trace metals by volcanic ash: The 2010 Eyjafjallajökull eruption,
1067 *Geochimica et Cosmochimica Acta*, 103, 138–160, <https://doi.org/10.1016/j.gca.2012.10.048>, 2013.
- 1068 Barreto, O.E. García, R. Román, M. Sicard, V. Rizi, R. Roininen, P.M Romero-Campos, Y. González, S.
1069 Rodríguez, R.D. García, C. Torres, M. Iarlori, E. Cuevas, C. Córdoba-Jabonero, J. de la Rosa, A. Rodríguez-
1070 Gómez, C. Muñoz-Porcar, A. Comerón, A. Bedoya-Velásquez, J.C. Antuña-Sanchez, V. Neustroev, E.
1071 Pietropaolo, Y. Lopez-Darias, M.A. López-Cayuela, C. Carvajal-Pérez, J.J. Bustos, O. Álvarez, C. Toledano, C.
1072 Aramo, J. Vilches, R. González, F.A. Almansa, R. Ceolato, N. Taquet, N. Prats, A. Redondas, C. Bayo, R.
1073 Ramos, V. Carreño, S.L. León, P.P. Rivas, A. Alcántara, C. López, P. Martín, La Palma Volcano Eruption:
1074 Characterisation of Volcanic Aerosols and Gas Emissions from a Synergetic Perspective, International
1075 Radiation Symposium (IRS), Thessaloniki (Greece), 4-8 July, 2022.
- 1076 Belart, J. M. C. and Pinel, V.: Pléiades co- and post-eruption survey in Cumbre Vieja volcano, La Palma, Spain
1077 (1), <https://doi.org/10.5281/ZENODO.5833771>, 2022.
- 1078 Birnbaum, J., Lev, E., Hernandez, P. A., Barrancos, J., Padilla, G. D., Asensio-Ramos, M., Calvo, D.,
1079 Rodríguez, F., Pérez, N. M., D'Auria, L., and Calvari, S.: Temporal variability of explosive activity at Tajogaite
1080 volcano, Cumbre Vieja (Canary Islands), 2021 eruption from ground-based infrared photography and
1081 videography, *Front. Earth Sci.*, 11, 1193436, <https://doi.org/10.3389/feart.2023.1193436>, 2023.
- 1082 Bluth, G. J. S., Casadevall, T. J., Schnetzler, C. C., Doiron, S. D., Walter, L. S., Krueger, A. J., and Badruddin,
1083 M.: Evaluation of sulfur dioxide emissions from explosive volcanism: the 1982–1983 eruptions of Galunggung,
1084 Java, Indonesia, *Journal of Volcanology and Geothermal Research*, 63, 243–256, [https://doi.org/10.1016/0377-](https://doi.org/10.1016/0377-0273(94)90077-9)
1085 [0273\(94\)90077-9](https://doi.org/10.1016/0377-0273(94)90077-9), 1994.
- 1086 Bonadonna, C., Pistolesi, M., Biass, S., Voloschina, M., Romero, J., Coppola, D., Folch, A., D'Auria, L.,
1087 Martin-Lorenzo, A., Dominguez, L., Pastore, C., Reyes Hardy, M., and Rodríguez, F.: Physical Characterization
1088 of Long-Lasting Hybrid Eruptions: The 2021 Tajogaite Eruption of Cumbre Vieja (La Palma, Canary islands),
1089 *JGR Solid Earth*, 127, e2022JB025302, <https://doi.org/10.1029/2022JB025302>, 2022.
- 1090 Bonadonna, C., Pistolesi, M., Dominguez, L., Freret-Lorgeril, V., Rossi, E., Fries, A., Biass, S., Voloschina, M.,
1091 Lemus, J., Romero, J. E., Zanon, V., Pastore, C., Reyes Hardy, M.-P., Di Maio, L. S., Gabellini, P., Martin-
1092 Lorenzo, A., Rodriguez, F., and Perez, N. M.: Tephra sedimentation and grainsize associated with pulsatory
1093 activity: the 2021 Tajogaite eruption of Cumbre Vieja (La Palma, Canary islands, Spain), *Front. Earth Sci.*, 11,
1094 1166073, <https://doi.org/10.3389/feart.2023.1166073>, 2023.
- 1095 Burrows, J. P., Richter, A., Dehn, A., Deters, B., Himmelmann, S., Voigt, S., and Orphal, J.: Atmospheric
1096 Remote-Sensing Reference Data From GOME-2. Temperature-dependent Absorption Cross-sections of O₃ in
1097 the 231–794 nm Range, *Journal of Quantitative Spectroscopy and Radiative Transfer*, 61, 509–517,
1098 [https://doi.org/10.1016/S0022-4073\(98\)00037-5](https://doi.org/10.1016/S0022-4073(98)00037-5), 1999.
- 1099 Burton, M., Aiuppa, A., Allard, P., Asensio-Ramos, M., Cofrades, A. P., La Spina, A., Nicholson, E. J., Zanon,
1100 V., Barrancos, J., Bitetto, M., Hartley, M., Romero, J. E., Waters, E., Stewart, A., Hernández, P. A., Lages, J. P.,
1101 Padrón, E., Wood, K., Esse, B., Hayer, C., Cyrzan, K., Rose-Koga, E. F., Schiavi, F., D'Auria, L., and Pérez, N.
1102 M.: Exceptional eruptive CO₂ emissions from intra-plate alkaline magmatism in the Canary volcanic
1103 archipelago, *Commun Earth Environ*, 4, 467, <https://doi.org/10.1038/s43247-023-01103-x>, 2023.
- 1104 Butz, A., Dinger, A. S., Bobrowski, N., Kostinek, J., Fieber, L., Fischerkeller, C., Giuffrida, G. B., Hase, F.,
1105 Klappenbach, F., Kuhn, J., Lübcke, P., Tirpitz, L., and Tu, Q.: Remote sensing of volcanic CO₂, HF, HCl, SO₂,
1106 and BrO in the downwind plume of Mt. Etna, *Atmos. Meas. Tech.*, 10, 1–14, [https://doi.org/10.5194/amt-10-1-](https://doi.org/10.5194/amt-10-1-2017)
1107 [2017](https://doi.org/10.5194/amt-10-1-2017), 2017.



- 1108 Cassidy, M., Iveson, A. A., Humphreys, M. C. S., Mather, T. A., Helo, C., Castro, J. M., Ruprecht, P., Pyle, D.
1109 M., and EIMF: Experimentally derived F, Cl, and Br fluid/melt partitioning of intermediate to silicic melts in
1110 shallow magmatic systems, *American Mineralogist*, 107, 1825–1839, <https://doi.org/10.2138/am-2022-8109>,
1111 2022.
- 1112 Charco, M., González, P. J., Pallero, J. L. G., García-Cañada, L., Del Fresno, C., and Rodríguez-Ortega, A.: The
1113 2021 La Palma (Canary islands) Eruption Ending Forecast Through Magma Pressure Drop, *Geophysical*
1114 *Research Letters*, 51, e2023GL106885, <https://doi.org/10.1029/2023GL106885>, 2024.
- 1115 Civico, R., Ricci, T., Scarlato, P., Taddeucci, J., Andronico, D., Del Bello, E., D’Auria, L., Hernández, P. A.,
1116 and Pérez, N. M.: High-resolution Digital Surface Model of the 2021 eruption deposit of Cumbre Vieja volcano,
1117 La Palma, Spain, *Sci Data*, 9, 435, <https://doi.org/10.1038/s41597-022-01551-8>, 2022.
- 1118 Copernicus EMSR546, [EMSR546 | Copernicus EMS On Demand Mapping](#)
- 1119 Coppola, D., Laiolo, M., Cigolini, C., Donne, D. D., and Ripepe, M.: Enhanced volcanic hot-spot detection
1120 using MODIS IR data: results from the MIROVA system, *SP*, 426, 181–205, <https://doi.org/10.1144/SP426.5>,
1121 2016.
- 1122 Córdoba-Jabonero, C., Sicard, M., Barreto, Á., Toledano, C., López-Cayuela, M. Á., Gil-Díaz, C., García, O.,
1123 Carvajal-Pérez, C. V., Comerón, A., Ramos, R., Muñoz-Porcar, C., and Rodríguez-Gómez, A.: Fresh volcanic
1124 aerosols injected in the atmosphere during the volcano eruptive activity at the Cumbre Vieja area (La Palma,
1125 Canary Islands): Temporal evolution and vertical impact, *Atmospheric Environment*, 300, 119667,
1126 <https://doi.org/10.1016/j.atmosenv.2023.119667>, 2023.
- 1127 Cuevas, E., Milford, C., Barreto, A., Bustos, J. J., García, O. E., García, R. D., Marrero, C., Prats, N., Ramos,
1128 R., Redondas, A., Reyes, E., Rivas-Soriano, P. P., Romero-Campos, P. M., Torres, C. J., Schneider, M., Yela,
1129 M., Belmonte, J., Almansa, F., López-Solano, C., Basart, S., Werner, E., Rodríguez, S., Alcántara, A., Alvarez,
1130 O., Bayo, C., Berjón, A., Borges, A., Carreño, V., Castro, N. J., China, N., Cruz, A. M., Damas, M., González,
1131 Y., Hernández, C., Hernández, J., León-Luís, S. F., López-Fernández, R., López-Solano, J., Mármol, I., Martín,
1132 T., Parra, F., Rodríguez-Valido, M., Sálamo, C., Santana, D., Santo-Tomás, F. and Serrano, A.: Izaña
1133 Atmospheric Research Center Activity Report 2021–2022. (Eds. Cuevas, E., Milford, C. and Tarasova, O.),
1134 State Meteorological Agency (AEMET), Madrid, Spain and World Meteorological Organization, Geneva,
1135 Switzerland, NIPO: 666-24-002-7, WMO/GAW Report No. 290, <https://doi.org/10.31978/666-24-002-7>, 2024.
- 1136
- 1137 Danckaert, T., Fayt, C., Van Roozendaal, M., De Smedt, I., Letocart, V., Merlaud, A., & Pinardi, G. (2014).
1138 *Qdoas Software User Manual, Version 2.108*.
- 1139
- 1140 D’Auria, L. and Martini, M.: Slug Flow: Modeling in a Conduit and Associated Elastic Radiation, in:
1141 *Encyclopedia of Complexity and Systems Science*, edited by: Meyers, R. A., Springer New York, New York,
1142 NY, 8153–8168, https://doi.org/10.1007/978-0-387-30440-3_483, 2009.
- 1143 D’Auria, L., Koulakov, I., Prudencio, J., Cabrera-Pérez, I., Ibáñez, J. M., Barrancos, J., García-Hernández, R.,
1144 Martínez Van Dorth, D., Padilla, G. D., Przeor, M., Ortega, V., Hernández, P., and Pérez, N. M.: Rapid magma
1145 ascent beneath La Palma revealed by seismic tomography, *Sci Rep*, 12, 17654, <https://doi.org/10.1038/s41598-022-21818-9>, 2022.
- 1146
- 1147 Day, J. M. D., Troll, V. R., Aulinas, M., Deegan, F. M., Geiger, H., Carracedo, J. C., Pinto, G. G., and Perez-
1148 Torrado, F. J.: Mantle source characteristics and magmatic processes during the 2021 La Palma eruption, *Earth*
1149 *and Planetary Science Letters*, 597, 117793, <https://doi.org/10.1016/j.epsl.2022.117793>, 2022.



- 1150 Dayton, K., Gazel, E., Wieser, P., Troll, V. R., Carracedo, J. C., La Madrid, H., Roman, D. C., Ward, J.,
1151 Aulinas, M., Geiger, H., Deegan, F. M., Gisbert, G., and Perez-Torrado, F. J.: Deep magma storage during the
1152 2021 La Palma eruption, *Sci. Adv.*, 9, eade7641, <https://doi.org/10.1126/sciadv.ade7641>, 2023.
- 1153 Dayton, K., Gazel, E., Wieser, P. E., Troll, V. R., Carracedo, J. C., Aulinas, M., and Perez-Torrado, F. J.:
1154 Magmatic Storage and Volatile Fluxes of the 2021 La Palma Eruption, *Geochem Geophys Geosyst*, 25,
1155 e2024GC011491, <https://doi.org/10.1029/2024GC011491>, 2024.
- 1156 Del Fresno, C., Cesca, S., Klügel, A., Domínguez Cerdeña, I., Díaz-Suárez, E. A., Dahm, T., García-Cañada, L.,
1157 Meletlidis, S., Milkereit, C., Valenzuela-Malebrán, C., López-Díaz, R., and López, C.: Magmatic plumbing and
1158 dynamic evolution of the 2021 La Palma eruption, *Nat Commun*, 14, 358, [https://doi.org/10.1038/s41467-023-](https://doi.org/10.1038/s41467-023-35953-y)
1159 35953-y, 2023.
- 1160 De Luca, C., Valerio, E., Giudicepietro, F., Macedonio, G., Casu, F., and Lanari, R.: Pre- and Co-Eruptive
1161 Analysis of the September 2021 Eruption at Cumbre Vieja Volcano (La Palma, Canary Islands) Through
1162 DInSAR Measurements and Analytical Modeling, *Geophysical Research Letters*, 49, e2021GL097293,
1163 <https://doi.org/10.1029/2021GL097293>, 2022.
- 1164 Duputel, Z., Ferrazzini, V., Journeau, C., Catherine, P., Kowalski, P., and Peltier, A.: Tracking changes in
1165 magma transport from very-long-period seismic signals at Piton de la Fournaise volcano, *Earth and Planetary*
1166 *Science Letters*, 620, 118323, <https://doi.org/10.1016/j.epsl.2023.118323>, 2023.
- 1167 EEA, 2023. European Union emission inventory report 1990-2021. EEA Report 04/2023,
1168 <https://doi.org/10.2800/68478>
- 1169 Ericksen, J., Fischer, T. P., Fricke, G. M., Nowicki, S., Pérez, N. M., Hernández Pérez, P., Padrón González, E.,
1170 and Moses, M. E.: Drone CO₂ measurements during the Tajogaite volcanic eruption, *Atmos. Meas. Tech.*, 17,
1171 4725–4736, <https://doi.org/10.5194/amt-17-4725-2024>, 2024.
- 1172 Feld, L., Herkommer, B., Vestner, J., Dubravica, D., Alberti, C., and Hase, F.: PROFFASTpylot: Running
1173 PROFFAST with Python, *JOSS*, 9, 6481, <https://doi.org/10.21105/joss.06481>, 2024.
- 1174 Fischer, T. P. and Aiuppa, A.: AGU Centennial Grand Challenge: Volcanoes and Deep Carbon Global CO₂
1175 Emissions From Subaerial Volcanism—Recent Progress and Future Challenges, *Geochem Geophys Geosyst*,
1176 21, e2019GC008690, <https://doi.org/10.1029/2019GC008690>, 2020.
- 1177 Frey, M., Sha, M. K., Hase, F., Kiel, M., Blumenstock, T., Harig, R., Surawicz, G., Deutscher, N. M., Shiomi,
1178 K., Franklin, J. E., Bösch, H., Chen, J., Grutter, M., Ohyama, H., Sun, Y., Butz, A., Mengistu Tsidu, G., Ene,
1179 D., Wunch, D., Cao, Z., Garcia, O., Ramonet, M., Vogel, F., and Orphal, J.: Building the COllaborative Carbon
1180 Column Observing Network (COCCON): long-term stability and ensemble performance of the EM27/SUN
1181 Fourier transform spectrometer, *Atmos. Meas. Tech.*, 12, 1513–1530, [https://doi.org/10.5194/amt-12-1513-](https://doi.org/10.5194/amt-12-1513-2019)
1182 2019, 2019.
- 1183 Galeczka, I., Oelkers, E. H., and Gislason, S. R.: The effect of the 2014-15 Bárðarbunga volcanic eruption on
1184 chemical denudation rates and the CO₂ budget, *Energy Procedia*, 146, 53–58,
1185 <https://doi.org/10.1016/j.egypro.2018.07.008>, 2018.
- 1186 García, O. E., Schneider, M., Sepúlveda, E., Hase, F., Blumenstock, T., Cuevas, E., Ramos, R., Gross, J.,
1187 Barthlott, S., Röhling, A. N., Sanromá, E., González, Y., Gómez-Peláez, Á. J., Navarro-Comas, M., Puente-dura,
1188 O., Yela, M., Redondas, A., Carreño, V., León-Luis, S. F., Reyes, E., García, R. D., Rivas, P. P., Romero-
1189 Campos, P. M., Torres, C., Prats, N., Hernández, M., and López, C.: Twenty years of ground-based NDACC
1190 FTIR spectrometry at Izaña Observatory – overview and long-term comparison to other techniques, *Atmos.*
1191 *Chem. Phys.*, 21, 15519–15554, <https://doi.org/10.5194/acp-21-15519-2021>, 2021.



- 1192 García, O. W. Stremme, N. Taquet, F. Hase, I. Ortega, J. Hannigan, D. Smale, C. Vigouroux, M. Grutter, T.
1193 Blumenstock, M. Schneider, A. Redondas. Sulphur dioxide from ground-based Fourier transform infrared
1194 spectroscopy: application to volcanic emissions, IRWG-NDACC Meeting 2022, 28 June-1 July, 2022.
- 1195 García, O., W. Stremme, N. Taquet, F. Hase, I. Ortega, J. Hannigan, C. Vigouroux, D. Smale, E. Mahieu, M.
1196 Grutter, N. Theys, T. Blumenstock, M. Schneider, and A. Redondas, Sulphur dioxide from ground-based
1197 Fourier transform infrared spectroscopy: application to volcanic emissions, in preparation.
- 1198 García, R. D., García, O. E., Cuevas-Agulló, E., Barreto, Á., Cachorro, V. E., Marrero, C., Almansa, F., Ramos,
1199 R., and Pó, M.: Spectral Aerosol Radiative Forcing and Efficiency of the La Palma Volcanic Plume over the
1200 Izaña Observatory, Remote Sensing, 15, 173, <https://doi.org/10.3390/rs15010173>, 2022.
- 1201 García-Gil, A., Jimenez, J., Marazuela, M. Á., Baquedano, C., Martínez-León, J., Cruz-Pérez, N., Laspidou, C.,
1202 and Santamarta, J. C.: Effects of the 2021 La Palma volcanic eruption on groundwater resources (part I):
1203 Hydraulic impacts, Groundwater for Sustainable Development, 23, 100989,
1204 <https://doi.org/10.1016/j.gsd.2023.100989>, 2023a.
- 1205 García-Gil, A., Jimenez, J., Gasco Cavero, S., Marazuela, M. Á., Baquedano, C., Martínez-León, J., Cruz-Pérez,
1206 N., Laspidou, C., and Santamarta, J. C.: Effects of the 2021 La Palma volcanic eruption on groundwater
1207 resources (part II): Hydrochemical impacts, Groundwater for Sustainable Development, 23, 100992,
1208 <https://doi.org/10.1016/j.gsd.2023.100992>, 2023b.
- 1209 Gennaro, E., Paonita, A., Iacono-Marziano, G., Moussallam, Y., Pichavant, M., Peters, N., and Martel, C.:
1210 Sulphur behaviour and redox conditions in etnean magmas during magma differentiation and degassing, Journal
1211 of Petrology, egaa095, <https://doi.org/10.1093/petrology/egaa095>, 2020.
- 1212 González, P.J.: Volcano-tectonic control of Cumbre Vieja. Science, 375, 1348-1349.
1213 <https://doi.org/10.1126/science.abn5148>, 2022.
- 1214 González-García, D., Boulesteix, T., Klügel, A., and Holtz, F.: Bubble-enhanced basanite–tephrite mixing in the
1215 early stages of the Cumbre Vieja 2021 eruption, La Palma, Canary islands, Sci Rep, 13, 14839,
1216 <https://doi.org/10.1038/s41598-023-41595-3>, 2023.
- 1217 Gordon, I. E., Rothman, L. S., Hargreaves, R. J., Hashemi, R., Karlovets, E. V., Skinner, F. M., Conway, E. K.,
1218 Hill, C., Kochanov, R. V., Tan, Y., Weislo, P., Finenko, A. A., Nelson, K., Bernath, P. F., Birk, M., Boudon, V.,
1219 Campargue, A., Chance, K. V., Coustenis, A., Drouin, B. J., Flaud, J. –M., Gamache, R. R., Hodges, J. T.,
1220 Jacquemart, D., Mlawer, E. J., Nikitin, A. V., Perevalov, V. I., Rotger, M., Tennyson, J., Toon, G. C., Tran, H.,
1221 Tyuterev, V. G., Adkins, E. M., Baker, A., Barbe, A., Canè, E., Császár, A. G., Dudaryonok, A., Egorov, O.,
1222 Fleisher, A. J., Fleurbaey, H., Foltynowicz, A., Furtenbacher, T., Harrison, J. J., Hartmann, J. –M., Horneman,
1223 V. –M., Huang, X., Karman, T., Karns, J., Kass, S., Kleiner, I., Kofman, V., Kwabia–Tchana, F., Lavrentieva,
1224 N. N., Lee, T. J., Long, D. A., Lukashevskaya, A. A., Lyulin, O. M., Makhnev, V. Yu., Matt, W., Massie, S. T.,
1225 Melosso, M., Mikhailenko, S. N., Mondelain, D., Müller, H. S. P., Naumenko, O. V., Perrin, A., Polyansky, O.
1226 L., Raddaoui, E., Raston, P. L., Reed, Z. D., Rey, M., Richard, C., Tóbiás, R., Sadiek, I., Schwenke, D. W.,
1227 Starikova, E., Sung, K., Tamassia, F., Tashkun, S. A., Vander Auwera, J., Vasilenko, I. A., Vidasin, A. A.,
1228 Villanueva, G. L., Vispoel, B., Wagner, G., Yachmenev, A., and Yurchenko, S. N.: The HITRAN2020
1229 molecular spectroscopic database, Journal of Quantitative Spectroscopy and Radiative Transfer, 277, 107949,
1230 <https://doi.org/10.1016/j.jqsrt.2021.107949>, 2022.
- 1231 Hansteen, T. H., Andersen, T., Neumann, E.-R., and Jelsma, H.: Fluid and silicate glass inclusions in ultramafic
1232 and mafic xenoliths from Hierro, Canary Islands: implications for mantle metasomatism, Contr. Mineral. and
1233 Petrol., 107, 242–254, <https://doi.org/10.1007/BF00310710>, 1991.



- 1234 Hansteen, T. H., Klügel, A., and Schmincke, H.-U.: Multi-stage magma ascent beneath the Canary Islands:
1235 evidence from fluid inclusions, *Contributions to Mineralogy and Petrology*, 132, 48–64,
1236 <https://doi.org/10.1007/s004100050404>, 1998.
- 1237 Harris, D. M. and Rose, W. I.: Dynamics of carbon dioxide emissions, crystallization, and magma ascent:
1238 hypotheses, theory, and applications to volcano monitoring at Mount St. Helens, *Bull Volcanol*, 58, 163–174,
1239 <https://doi.org/10.1007/s004450050133>, 1996.
- 1240 Hase, F., Hannigan, J. W., Coffey, M. T., Goldman, A., Höpfner, M., Jones, N. B., Rinsland, C. P., and Wood,
1241 S. W.: Intercomparison of retrieval codes used for the analysis of high-resolution, ground-based FTIR
1242 measurements, *Journal of Quantitative Spectroscopy and Radiative Transfer*, 87, 25–52,
1243 <https://doi.org/10.1016/j.jqsrt.2003.12.008>, 2004.
- 1244 Hayer, C., Burton, M., Ferrazzini, V., Esse, B., and Di Muro, A.: Unusually high SO₂ emissions and plume
1245 height from Piton de la Fournaise volcano during the April 2020 eruption, *Bull Volcanol*, 85, 21,
1246 <https://doi.org/10.1007/s00445-023-01628-1>, 2023.
- 1247 Hedelt, P., Reichardt, J., Lauermann, F., Weiß, B., Theys, N., Redondas, A., Barreto, A., Garcia, O., and
1248 Loyola, D.: Analysis of the long-range transport of the volcanic plume from the 2021 Tajogaite/Cumbre Vieja
1249 eruption to Europe using TROPOMI and ground-based measurements, *Atmos. Chem. Phys.*, 25, 1253–1272,
1250 <https://doi.org/10.5194/acp-25-1253-2025>, 2025.
- 1251
1252 Herkommer, B., Alberti, C., Castracane, P., Chen, J., Dehn, A., Dietrich, F., Deutscher, N. M., Frey, M. M.,
1253 Groß, J., Gillespie, L., Hase, F., Morino, I., Pak, N. M., Walker, B., and Wunch, D.: Using a portable FTIR
1254 spectrometer to evaluate the consistency of Total Carbon Column Observing Network (TCCON) measurements
1255 on a global scale: the Collaborative Carbon Column Observing Network (COCCON) travel standard, *Atmos.*
1256 *Meas. Tech.*, 17, 3467–3494, <https://doi.org/10.5194/amt-17-3467-2024>, 2024a.
- 1257 Herkommer, B.: Improving the consistency of greenhouse gas measurements from ground-based remote sensing
1258 instruments using a portable FTIR spectrometer, <https://doi.org/10.5445/IR/1000168723>, 2024b.
- 1259
1260 Jarosewich, E., Nelen, J. A., and Norberg, J. A.: Reference Samples for Electron Microprobe Analysis*,
1261 *Geostandards Newsletter*, 4, 43–47, <https://doi.org/10.1111/j.1751-908X.1980.tb00273.x>, 1980.
- 1262 Jiménez, J., Gasco Caverro, S., Marazuela, M. Á., Baquedano, C., Lapidou, C., Santamarta, J. C., and García-
1263 Gil, A.: Effects of the 2021 La Palma volcanic eruption on groundwater hydrochemistry: Geochemical
1264 modelling of endogenous CO₂ release to surface reservoirs, water-rock interaction and influence of thermal and
1265 seawater, *Science of The Total Environment*, 929, 172594, <https://doi.org/10.1016/j.scitotenv.2024.172594>,
1266 2024.
- 1267 Kern, C., Lerner, A. H., Elias, T., Nadeau, P. A., Holland, L., Kelly, P. J., Werner, C. A., Clor, L. E., and
1268 Cappos, M.: Quantifying gas emissions associated with the 2018 rift eruption of Kīlauea Volcano using ground-
1269 based DOAS measurements, *Bull Volcanol*, 82, 55, <https://doi.org/10.1007/s00445-020-01390-8>, 2020.
- 1270 Klügel, A., Hoernle, K. A., Schmincke, H., and White, J. D. L.: The chemically zoned 1949 eruption on La
1271 Palma (Canary islands): Petrologic evolution and magma supply dynamics of a rift zone eruption, *J. Geophys.*
1272 *Res.*, 105, 5997–6016, <https://doi.org/10.1029/1999JB900334>, 2000.
- 1273 Spina, A. L., Burton, M., Salerno, G., and Caltabiano, T.: Insights into magma dynamics at Etna (Sicily) from
1274 SO₂ and HCl fluxes during the 2008–2009 eruption, *Geology*, 51, 419–423, <https://doi.org/10.1130/G50707.1>,
1275 2023.



- 1276 Lo Forte, F. M., Schiavi, F., Rose-Koga, E. F., Rotolo, S. G., Verdier-Paoletti, M., Aiuppa, A., and Zanon, V.:
1277 High CO₂ in the mantle source of ocean island basanites, *Geochimica et Cosmochimica Acta*, 368, 93–111,
1278 <https://doi.org/10.1016/j.gca.2024.01.016>, 2024.
- 1279 Longpré, M.-A., Stix, J., Klügel, A., and Shimizu, N.: Mantle to surface degassing of carbon- and sulphur-rich
1280 alkaline magma at El Hierro, Canary Islands, *Earth and Planetary Science Letters*, 460, 268–280,
1281 <https://doi.org/10.1016/j.epsl.2016.11.043>, 2017.
- 1282 Longpré, M.-A., Tramontano, S., Pankhurst, M. J., Roman, D. C., Reiss, M. C., Cortese, F., James, M. R.,
1283 Spina, L., Rodríguez, F., Coldwell, B., Martín-Lorenzo, A., Barbee, O., D’Auria, L., Chamberlain, K. J., and
1284 Scarrow, J. H.: Shifting melt composition linked to volcanic tremor at Cumbre Vieja volcano, *Nat. Geosci.*,
1285 <https://doi.org/10.1038/s41561-024-01623-x>, 2025.
- 1286 Mather, T. A., Witt, M. L. I., Pyle, D. M., Quayle, B. M., Aiuppa, A., Bagnato, E., Martin, R. S., Sims, K. W.
1287 W., Edmonds, M., Sutton, A. J., and Ilyinskaya, E.: Halogens and trace metal emissions from the ongoing 2008
1288 summit eruption of Kīlauea volcano, Hawai‘i, *Geochimica et Cosmochimica Acta*, 83, 292–323,
1289 <https://doi.org/10.1016/j.gca.2011.11.029>, 2012.
- 1290 Mezcuá, J. and Rueda, J.: Seismic swarms and earthquake activity b-value related to the September 19, 2021, La
1291 Palma volcano eruption in Cumbre Vieja, Canary islands (Spain), *Bull Volcanol*, 85, 32,
1292 <https://doi.org/10.1007/s00445-023-01646-z>, 2023.
- 1293 Milford, C.: Izaña Atmospheric Research Center. Activity Report 2021-2022, edited by: Cuevas Agulló, E. and
1294 Tarasova, O., Agencia Estatal de Meteorología; Organización Meteorológica Mundial,
1295 <https://doi.org/10.31978/666-24-002-7>, 2024.
- 1296 Milford, C., Torres, C., Vilches, J., Gossman, A.-K., Weis, F., Suárez-Molina, D., García, O. E., Prats, N.,
1297 Barreto, Á., García, R. D., Bustos, J. J., Marrero, C. L., Ramos, R., Chinea, N., Boulesteix, T., Taquet, N.,
1298 Rodríguez, S., López-Darias, J., Sicard, M., Córdoba-Jabonero, C., and Cuevas, E.: Impact of the 2021 La
1299 Palma volcanic eruption on air quality: Insights from a multidisciplinary approach, *Science of The Total*
1300 *Environment*, 869, 161652, <https://doi.org/10.1016/j.scitotenv.2023.161652>, 2023.
- 1301 MITECO, (2023). Inventory Informative Report (Informe de Inventario de Emisiones de Contaminantes a la
1302 Atmósfera), Ministerio para la Transición Ecológica y el Reto Demográfico Secretaría General Técnica. Centro
1303 de Publicaciones (2023), [https://www.miteco.gob.es/content/dam/miteco/es/calidad-y-evaluacion-](https://www.miteco.gob.es/content/dam/miteco/es/calidad-y-evaluacion-ambiental/temas/sistema-espanol-de-inventario-sei-es_iir_edicion2023_tcm30-560375.pdf)
1304 [ambiental/temas/sistema-espanol-de-inventario-sei-es_iir_edicion2023_tcm30-560375.pdf](https://www.miteco.gob.es/content/dam/miteco/es/calidad-y-evaluacion-ambiental/temas/sistema-espanol-de-inventario-sei-es_iir_edicion2023_tcm30-560375.pdf)
- 1305 Muñoz, V., Walter, T. R., Zorn, E. U., Shevchenko, A. V., González, P. J., Reale, D., and Sansosti, E.: Satellite
1306 Radar and Camera Time Series Reveal Transition from Aligned to Distributed Crater Arrangement during the
1307 2021 Eruption of Cumbre Vieja, La Palma (Spain), *Remote Sensing*, 14, 6168,
1308 <https://doi.org/10.3390/rs14236168>, 2022.
- 1309 Oppenheimer, C., Francis, P., Burton, M., Maciejewski, A. J. H., & Boardman, L. (1998). Remote measurement
1310 of volcanic gases by Fourier transform infrared spectroscopy. *Applied Physics B: Lasers & Optics*, 67(4).
- 1311 Padrón, E., Pérez, N. M., Hernández, P. A., Sumino, H., Melián, G. V., Alonso, M., Rodríguez, F., Asensio-
1312 Ramos, M., and D’Auria, L.: Early Precursory Changes in the ³He/⁴He Ratio Prior to the 2021 Tajogaite
1313 Eruption at Cumbre Vieja Volcano, La Palma, Canary Islands, *Geophysical Research Letters*, 49,
1314 e2022GL099992, <https://doi.org/10.1029/2022GL099992>, 2022.
- 1315 Pankhurst, M. J., Scarrow, J. H., Barbee, O. A., Hickey, J., Coldwell, B. C., Rollinson, G. K., Rodríguez-
1316 Losada, J. A., Martín Lorenzo, A., Rodríguez, F., Hernández, W., Calvo Fernández, D., Hernández, P. A., and



- 1317 Pérez, N. M.: Rapid response petrology for the opening eruptive phase of the 2021 Cumbre Vieja eruption, La
1318 Palma, Canary Islands, *Volcanica*, 5, 1–10, <https://doi.org/10.30909/vol.05.01.0110>, 2022.
- 1319 PEVOLCA 2021. Scientific Committee Report 25/12/2021: Actualización de la actividad volcánica en Cumbre
1320 Vieja (La Palma)(2021). <https://info.igme.es/eventos/Erupcion-volcanica-la-palma/pevolca>
- 1321 Platt, U. and Stutz, J.: Differential Absorption Spectroscopy, in: *Differential Optical Absorption Spectroscopy*,
1322 Springer Berlin Heidelberg, Berlin, Heidelberg, 135–174, https://doi.org/10.1007/978-3-540-75776-4_6, 2008.
- 1323 Pfeffer, M., Bergsson, B., Barsotti, S., Stefánsdóttir, G., Galle, B., Arellano, S., Conde, V., Donovan, A.,
1324 Ilyinskaya, E., Burton, M., Aiuppa, A., Whitty, R., Simmons, I., Arason, P., Jónasdóttir, E., Keller, N., Yeo, R.,
1325 Arngrímsson, H., Jóhannsson, P., Butwin, M., Askew, R., Dumont, S., Von Löwis, S., Ingvarsson, P., La Spina,
1326 A., Thomas, H., Prata, F., Grassa, F., Giudice, G., Stefánsson, A., Marzano, F., Montopoli, M., and Mereu, L.:
1327 Ground-Based Measurements of the 2014–2015 Holuhraun Volcanic Cloud (Iceland), *Geosciences*, 8, 29,
1328 <https://doi.org/10.3390/geosciences8010029>, 2018.
- 1329 Plank, S., Shevchenko, A. V., d’Angelo, P., Gstaiger, V., González, P. J., Cesca, S., Martinis, S., and Walter, T.
1330 R.: Combining thermal, tri-stereo optical and bi-static InSAR satellite imagery for lava volume estimates: the
1331 2021 Cumbre Vieja eruption, La Palma, *Sci Rep*, 13, 2057, <https://doi.org/10.1038/s41598-023-29061-6>, 2023.
- 1332 Powers, J. G., Klemp, J. B., Skamarock, W. C., Davis, C. A., Dudhia, J., Gill, D. O., Coen, J. L., Gochis, D. J.,
1333 Ahmadv, R., Peckham, S. E., Grell, G. A., Michalakes, J., Trahan, S., Benjamin, S. G., Alexander, C. R.,
1334 Dimego, G. J., Wang, W., Schwartz, C. S., Romine, G. S., Liu, Z., Snyder, C., Chen, F., Barlage, M. J., Yu, W.,
1335 and Duda, M. G.: The Weather Research and Forecasting Model: Overview, System Efforts, and Future
1336 Directions, *Bulletin of the American Meteorological Society*, 98, 1717–1737, [https://doi.org/10.1175/BAMS-D-](https://doi.org/10.1175/BAMS-D-15-00308.1)
1337 [15-00308.1](https://doi.org/10.1175/BAMS-D-15-00308.1), 2017.
- 1338 Rivalta, E. and Segall, P.: Magma compressibility and the missing source for some dike intrusions, *Geophysical*
1339 *Research Letters*, 35, 2007GL032521, <https://doi.org/10.1029/2007GL032521>, 2008.
- 1340 Rodgers, C. D.: *Inverse Methods for Atmospheric Sounding: Theory and Practice*, WORLD SCIENTIFIC,
1341 <https://doi.org/10.1142/3171>, 2000.
- 1342 Rodríguez, S., Alastuey, A., and Querol, X.: A review of methods for long term in situ characterization of
1343 aerosol dust, *Aeolian Research*, 6, 55–74, <https://doi.org/10.1016/j.aeolia.2012.07.004>, 2012.
- 1344 Rodríguez, R., López Darias, J., de la Rosa, J., Vilches, J., Boulesteix, T., Taquet, N., Belbachir, I., Villena-
1345 Armas, G., Sánchez de La Campa, A.M., García, O., Ayala, J. H. Ashes, trace gases and the composition of the
1346 resulting volcanic aerosols during the 2021 eruption at La Palma – Canary Islands, submitted to ACP.
- 1347 Román, R., González, R., Antuña-Sánchez, J.C., Barreto, A., Martín, P., Toledano, C., Ramos, R., Cazorla, A.,
1348 Herrero-Anta, S., Mateos, D., García, O., González-Fernández, D., Carracedo, R., Herreras-Giralda, M.,
1349 Carreño, V., Calle, A., Cachorro, V.E., Cuevas, E., de Frutos, A.M.: Vertical profiles of aerosol properties
1350 retrieved at La Palma, Canary islands, during the Cumbre-Vieja volcano eruption in September-October 2021,
1351 *European Lidar Conference (ELC)*, Granada, 16-18 November, 2021.
- 1352 Romero, J. E., Burton, M., Cáceres, F., Taddeucci, J., Civico, R., Ricci, T., Pankhurst, M. J., Hernández, P. A.,
1353 Bonadonna, C., Llewellyn, E. W., Pistolesi, M., Polacci, M., Solana, C., D’Auria, L., Arzilli, F., Andronico, D.,
1354 Rodríguez, F., Asensio-Ramos, M., Martín-Lorenzo, A., Hayer, C., Scarlato, P., and Perez, N. M.: The initial
1355 phase of the 2021 Cumbre Vieja ridge eruption (Canary islands): Products and dynamics controlling edifice
1356 growth and collapse, *Journal of Volcanology and Geothermal Research*, 431, 107642,
1357 <https://doi.org/10.1016/j.jvolgeores.2022.107642>, 2022.



- 1358 Rose-Koga, E. F., Bouvier, A.-S., Gaetani, G. A., Wallace, P. J., Allison, C. M., Andrys, J. A., Angeles De La
1359 Torre, C. A., Barth, A., Bodnar, R. J., Bracco Gartner, A. J. J., Butters, D., Castillejo, A., Chilson-Parks, B.,
1360 Choudhary, B. R., Cluzel, N., Cole, M., Cottrell, E., Daly, A., Danyushevsky, L. V., DeVitre, C. L., Drignon,
1361 M. J., France, L., Gaborieau, M., Garcia, M. O., Gatti, E., Genske, F. S., Hartley, M. E., Hughes, E. C., Iveson,
1362 A. A., Johnson, E. R., Jones, M., Kagoshima, T., Katzir, Y., Kawaguchi, M., Kawamoto, T., Kelley, K. A.,
1363 Koornneef, J. M., Kurz, M. D., Laubier, M., Layne, G. D., Lerner, A., Lin, K.-Y., Liu, P.-P., Lorenzo-Merino,
1364 A., Luciani, N., Magalhães, N., Marschall, H. R., Michael, P. J., Monteleone, B. D., Moore, L. R.,
1365 Moussallam, Y., Muth, M., Myers, M. L., Narváez, D. F., Navon, O., Newcombe, M. E., Nichols, A. R. L.,
1366 Nielsen, R. L., Pamukcu, A., Plank, T., Rasmussen, D. J., Roberge, J., Schiavi, F., Schwartz, D., Shimizu, K.,
1367 Shimizu, K., Shimizu, N., Thomas, J. B., Thompson, G. T., Tucker, J. M., Ustunisik, G., Waelkens, C., Zhang,
1368 Y., and Zhou, T.: Silicate melt inclusions in the new millennium: A review of recommended practices for
1369 preparation, analysis, and data presentation, *Chemical Geology*, 570, 120145,
1370 <https://doi.org/10.1016/j.chemgeo.2021.120145>, 2021.
- 1371 Ruggieri, F., Forte, G., Bocca, B., Casentini, B., Bruna Petrangeli, A., Salatino, A., and Gimeno, D.: Potentially
1372 harmful elements released by volcanic ash of the 2021 Tajogaite eruption (Cumbre Vieja, La Palma Island,
1373 Spain): Implications for human health, *Science of The Total Environment*, 905, 167103,
1374 <https://doi.org/10.1016/j.scitotenv.2023.167103>, 2023.
- 1375 Sánchez-España, J., Mata, M. P., Vegas, J., Lozano, G., Mediato, J., Martínez Martínez, J., Galindo, I., Sánchez,
1376 N., Del Moral, B., Ordóñez, B., De Vergara, A., Nieto, A., Andrés, M., Vázquez, I., Bellido, E., and Castillo-
1377 Carrión, M.: Leaching tests reveal fast aluminum fluoride release from ashfall accumulated in La Palma (Canary
1378 Islands, Spain) after the 2021 Tajogaite eruption, *Journal of Volcanology and Geothermal Research*, 444,
1379 107959, <https://doi.org/10.1016/j.jvolgeores.2023.107959>, 2023.
- 1380 Saumur, B. M., Cruden, A. R., and Boutelier, D.: Sulfide Liquid Entrainment by Silicate Magma: Implications
1381 for the Dynamics and Petrogenesis of Magmatic Sulfide Deposits, *J. Petrology*, 56, 2473–2490,
1382 <https://doi.org/10.1093/petrology/egv080>, 2015.
- 1383 Schneider, M., Blumenstock, T., Chipperfield, M. P., Hase, F., Kouker, W., Reddmann, T., Ruhnke, R., Cuevas,
1384 E., and Fischer, H.: Subtropical trace gas profiles determined by ground-based FTIR spectroscopy at Izaña (28°
1385 N, 16° W): Five-year record, error analysis, and comparison with 3-D CTMs, *Atmos. Chem. Phys.*, 5, 153–167,
1386 <https://doi.org/10.5194/acp-5-153-2005>, 2005.
- 1387 Seinfeld, J. H. and Pandis, S. N.: *Atmospheric chemistry and physics: from air pollution to climate change*,
1388 Wiley, New York Weinheim, 1326 pp., 1998.
- 1389 Shinohara, H., Kazahaya, K., Saito, G., Fukui, K., and Odai, M.: Variation of CO₂/SO₂ ratio in volcanic plumes
1390 of Miyakejima: Stable degassing deduced from heliborne measurements, *Geophysical Research Letters*, 30,
1391 2002GL016105, <https://doi.org/10.1029/2002GL016105>, 2003.
- 1392 Shinohara, H., Aiuppa, A., Giudice, G., Gurrieri, S., and Liuzzo, M.: Variation of H₂O/CO₂ and CO₂/SO₂ ratios
1393 of volcanic gases discharged by continuous degassing of Mount Etna volcano, Italy, *J. Geophys. Res.*, 113,
1394 2007JB005185, <https://doi.org/10.1029/2007JB005185>, 2008.
- 1395 Skamarock, W. C., Klemp, J. B., Dudhia, J., Gill, D. O., Liu, Z., Berner, J., Wang, W., Powers, J. G., Duda, M.
1396 G., Barker, D. M., and Huang, X.-Y.: A Description of the Advanced Research WRF Model Version 4,
1397 UCAR/NCAR, <https://doi.org/10.5065/1DFH-6P97>, 2019.
- 1398 Smale, D., Hannigan, J. W., Lad, S., Murphy, M., McGaw, J., and Robinson, J.: Opportunistic observations of
1399 Mount Erebus volcanic plume HCl, HF and SO₂ by high resolution solar occultation mid infra-red spectroscopy,



- 1400 Journal of Quantitative Spectroscopy and Radiative Transfer, 307, 108665,
1401 <https://doi.org/10.1016/j.jqsrt.2023.108665>, 2023.
- 1402 Spina, A. L., Burton, M., Salerno, G., and Caltabiano, T.: Insights into magma dynamics at Etna (Sicily) from
1403 SO₂ and HCl fluxes during the 2008–2009 eruption, *Geology*, 51, 419–423, <https://doi.org/10.1130/G50707.1>,
1404 2023.
- 1405 Stremme, W., Grutter, M., Baylón, J., Taquet, N., Bezanilla, A., Plaza-Medina, E., Schiavo, B., Rivera, C.,
1406 Blumenstock, T., and Hase, F.: Direct solar FTIR measurements of CO₂ and HCl in the plume of Popocatepetl
1407 Volcano, Mexico, *Front. Earth Sci.*, 11, 1022976, <https://doi.org/10.3389/feart.2023.1022976>, 2023.
- 1408 Taquet, N., Stremme, W., Grutter, M., Baylón, J., Bezanilla, A., Schiavo, B., Rivera, C., Campion, R.,
1409 Boulesteix, T., Nieto-Torres, A., Espinasa-Pereña, R., Blumenstock, T., and Hase, F.: Variability in the Gas
1410 Composition of the Popocatepetl Volcanic Plume, *Front. Earth Sci.*, 7, 114,
1411 <https://doi.org/10.3389/feart.2019.00114>, 2019.
- 1412 Taquet, N., Rivera Cárdenas, C., Stremme, W., Boulesteix, T., Bezanilla, A., Grutter, M., García, O., Hase, F.,
1413 and Blumenstock, T.: Combined direct-sun ultraviolet and infrared spectroscopies at Popocatepetl volcano
1414 (Mexico), *Front. Earth Sci.*, 11, 1062699, <https://doi.org/10.3389/feart.2023.1062699>, 2023.
- 1415 Taracsák, Z., Hartley, M. E., Burgess, R., Edmonds, M., Iddon, F., and Longpré, M.-A.: High fluxes of deep
1416 volatiles from ocean island volcanoes: Insights from El Hierro, Canary Islands, *Geochimica et Cosmochimica*
1417 *Acta*, 258, 19–36, <https://doi.org/10.1016/j.gca.2019.05.020>, 2019.
- 1418 Theys, N., Fioletov, V., Li, C., De Smedt, I., Lerot, C., McLinden, C., Krotkov, N., Griffin, D., Clarisse, L.,
1419 Hedelt, P., Loyola, D., Wagner, T., Kumar, V., Innes, A., Ribas, R., Hendrick, F., Vlietinck, J., Brenot, H., and
1420 Van Roozendael, M.: A sulfur dioxide Covariance-Based Retrieval Algorithm (COBRA): application to
1421 TROPOMI reveals new emission sources, *Atmos. Chem. Phys.*, 21, 16727–16744, [https://doi.org/10.5194/acp-](https://doi.org/10.5194/acp-21-16727-2021)
1422 21-16727-2021, 2021.
- 1423 Torres-González, P. A., Luengo-Oroz, N., Lamolda, H., D'Alessandro, W., Albert, H., Iribarren, I., Moure-
1424 García, D., and Soler, V.: Unrest signals after 46 years of quiescence at Cumbre Vieja, La Palma, Canary
1425 islands, *Journal of Volcanology and Geothermal Research*, 392, 106757,
1426 <https://doi.org/10.1016/j.jvolgeores.2019.106757>, 2020.
- 1427 Ubide, T., Márquez, Á., Ancochea, E., Huertas, M. J., Herrera, R., Coello-Bravo, J. J., Sanz-Mangas, D.,
1428 Mulder, J., MacDonald, A., and Galindo, I.: Discrete magma injections drive the 2021 La Palma eruption, *Sci.*
1429 *Adv.*, 9, eadg4813, <https://doi.org/10.1126/sciadv.adg4813>, 2023.
- 1430 Valade, S., Ley, A., Massimetti, F., D'Hondt, O., Laiolo, M., Coppola, D., Loibl, D., Hellwich, O., and Walter,
1431 T. R.: Towards Global Volcano Monitoring Using Multisensor Sentinel Missions and Artificial Intelligence:
1432 The MOUNTS Monitoring System, *Remote Sensing*, 11, 1528, <https://doi.org/10.3390/rs11131528>, 2019.
- 1433 Vandaele, A. C., Hermans, C., and Fally, S.: Fourier transform measurements of SO₂ absorption cross sections:
1434 II., *Journal of Quantitative Spectroscopy and Radiative Transfer*, 110, 2115–2126,
1435 <https://doi.org/10.1016/j.jqsrt.2009.05.006>, 2009.
- 1436 Van Gerve, T. D., Neave, D. A., Wieser, P., Lamadrid, H., Hulsbosch, N., and Namur, O.: The Origin and
1437 Differentiation of CO₂-Rich Primary Melts in Ocean Island Volcanoes: Integrating 3D X-Ray Tomography
1438 with Chemical Microanalysis of Olivine-Hosted Melt Inclusions from Pico (Azores)., *Journal of Petrology*, 65,
1439 egae006, <https://doi.org/10.1093/petrology/egae006>, 2024.



- 1440 Vasileva, A., Moiseenko, K., Skorokhod, A., Belikov, I., Kopeikin, V., and Lavrova, O.: Emission ratios of
1441 trace gases and particles for Siberian forest fires on the basis of mobile ground observations, *Atmos. Chem.*
1442 *Phys.*, 17, 12303–12325, <https://doi.org/10.5194/acp-17-12303-2017>, 2017.
- 1443 Voigt, C., Jessberger, P., Jurkat, T., Kaufmann, S., Baumann, R., Schlager, H., Bobrowski, N., Giuffrida, G.,
1444 and Salerno, G.: Evolution of CO₂, SO₂, HCl, and HNO₃ in the volcanic plumes from Etna, *Geophys. Res. Lett.*,
1445 41, 2196–2203, <https://doi.org/10.1002/2013GL058974>, 2014.
- 1446 Walter, T. R., Zorn, E. U., González, P. J., Sansosti, E., Muñoz, V., Shevchenko, A. V., Plank, S. M., Reale, D.
1447 and Richter, N.: Late complex tensile fracturing interacts with topography at Cumbre Vieja, La Palma,
1448 *Volcanica*, 6(1), pp. 1–17. <https://doi.org/10.30909/vol.06.01.0117>, 2023.
- 1449 Wardell, L. J., Kyle, P. R., and Chaffin, C.: Carbon dioxide and carbon monoxide emission rates from an
1450 alkaline intra-plate volcano: Mt. Erebus, Antarctica, *Journal of Volcanology and Geothermal Research*, 131,
1451 109–121, [https://doi.org/10.1016/S0377-0273\(03\)00320-2](https://doi.org/10.1016/S0377-0273(03)00320-2), 2004.
- 1452 Werner, C., Evans, W. C., Kelly, P. J., McGimsey, R., Pfeffer, M., Doukas, M., and Neal, C.: Deep magmatic
1453 degassing versus scrubbing: Elevated CO₂ emissions and C/S in the lead-up to the 2009 eruption of Redoubt
1454 Volcano, Alaska, *Geochim Geophys Geosyst*, 13, 2011GC003794, <https://doi.org/10.1029/2011GC003794>,
1455 2012.
- 1456 WMO, 2018: 19th WMO/IAEA Meeting on Carbon Dioxide, Other Greenhouse Gases and Related Tracers
1457 Measurement Techniques (GGMT-2017), Dübendorf, Switzerland, 27–31 August 2017, GAW Report No. 242,
1458 World Meteorological Organization, Geneva, Switzerland.
- 1459 Wunch, D., Toon, G. C., Blavier, J. F. L., Washenfelder, R. A., Notholt, J., Connor, B. J., Griffith, D. W. T.,
1460 Sherlock, V., and Wennberg, P. O.: The total carbon column observing network, *Philos. T. R. Soc. A*, 369,
1461 2087–2112, 2011.
- 1462 Yokelson, R. J., Karl, T., Artaxo, P., Blake, D. R., Christian, T. J., Griffith, D. W. T., Guenther, A., and Hao, W.
1463 M.: The Tropical Forest and Fire Emissions Experiment: overview and airborne fire emission factor
1464 measurements, *Atmos. Chem. Phys.*, 7, 5175–5196, <https://doi.org/10.5194/acp-7-5175-2007>, 2007.
- 1465 Zhang, C., Koepke, J., Wang, L., Wolff, P. E., Wilke, S., Stechern, A., Almeev, R., and Holtz, F.: A Practical
1466 Method for Accurate Measurement of Trace Level Fluorine in Mg- and Fe-Bearing Minerals and Glasses Using
1467 Electron Probe Microanalysis, *Geostandard Geoanalytic Res.*, 40, 351–363, <https://doi.org/10.1111/j.1751-908X.2015.00390.x>, 2016.
- 1469 Zhang, B., Shen, H., Yun, X., Zhong, Q., Henderson, B. H., Wang, X., Shi, L., Gunthe, S. S., Huey, L. G., Tao,
1470 S., Russell, A. G., and Liu, P.: Global Emissions of Hydrogen Chloride and Particulate Chloride from
1471 Continental Sources, *Environ. Sci. Technol.*, 56, 3894–3904, <https://doi.org/10.1021/acs.est.1c05634>, 2022.